Title

Niemann-Pick Type C Disease Reveals a Link between Lysosomal Cholesterol and PtdIns(4,5)P 2 That Regulates Neuronal Excitability

Journal

Cell Reports, 27(9)

ISSN

2639-1856

Authors

Vivas, Oscar
Tiscione, Scott A
Dixon, Rose E
et al.

Publication Date

2019-05-01

DOI

10.1016/j.celrep.2019.04.099

Peer reviewed

HHS Public Access

Author manuscript

Cell Rep. Author manuscript; available in PMC 2019 June 06.

Published in final edited form as:

Cell Rep. 2019 May 28; 27(9): 2636–2648.e4. doi:10.1016/j.celrep.2019.04.099.

Niemann-Pick Type C Disease Reveals a Link between Lysosomal Cholesterol and PtdIns(4,5)P_2 That Regulates Neuronal Excitability

Oscar Vivas[1], **Scott A. Tiscione**[1], **Rose E. Dixon**[1], **Daniel S. Ory**[2], and **Eamonn J. Dickson**[1,3,*]

[1]Department of Physiology and Membrane Biology, University of California, Davis, Davis, CA 95616, USA

[2]Department of Internal Medicine, Washington University School of Medicine, St. Louis, MO 63110, USA

[3]Lead Contact

SUMMARY

There is increasing evidence that the lysosome is involved in the pathogenesis of a variety of neurodegenerative disorders. Thus, mechanisms that link lysosome dysfunction to the disruption of neuronal homeostasis offer opportunities to understand the molecular underpinnings of neurodegeneration and potentially identify specific therapeutic targets. Here, using a monogenic neurodegenerative disorder, NPC1 disease, we demonstrate that reduced cholesterol efflux from lysosomes aberrantly modifies neuronal firing patterns. The molecular mechanism linking alterations in lysosomal cholesterol egress to intrinsic tuning of neuronal excitability is a transcriptionally mediated upregulation of the ABCA1 transporter, whose PtdIns(4,5)P_2-floppase activity decreases plasma membrane PtdIns(4,5)P_2. The consequence of reduced PtdIns(4,5)P_2 is a parallel decrease in a key regulator of neuronal excitability, the voltage-gated KCNQ2/3 potassium channel, which leads to hyperexcitability in NPC1 disease neurons. Thus, cholesterol efflux from lysosomes regulates PtdIns(4,5)P_2 to shape the electrical and functional identity of the plasma membrane of neurons in health and disease.

In Brief

*Correspondence: ejdickson@ucdavis.edu.

AUTHOR CONTRIBUTIONS

O.V. and E.J.D. designed the experiments. O.V. collected and analyzed the electrophysiology and imaging data. O.V. and S.A.T. collected and analyzed the western blot data. E.J.D. collected and analyzed the MS data. O.V. and E.J.D. wrote the manuscript, with input from all of the authors.

DECLARATION OF INTERESTS

The authors declare no competing interests.

SUPPLEMENTAL INFORMATION

Supplemental Information can be found online at https://doi.org/10.1016/j.celrep.2019.04.099.

NPC1 disease is a neurodegenerative disorder that occurs due to mutations in the lysosomal NPC1 cholesterol transporter. Vivas et al. define steps in the pathogenic cascade, downstream of lysosomal cholesterol accumulation, that lead to hyperexcitability in NPC1 disease neurons.

Graphical Abstract

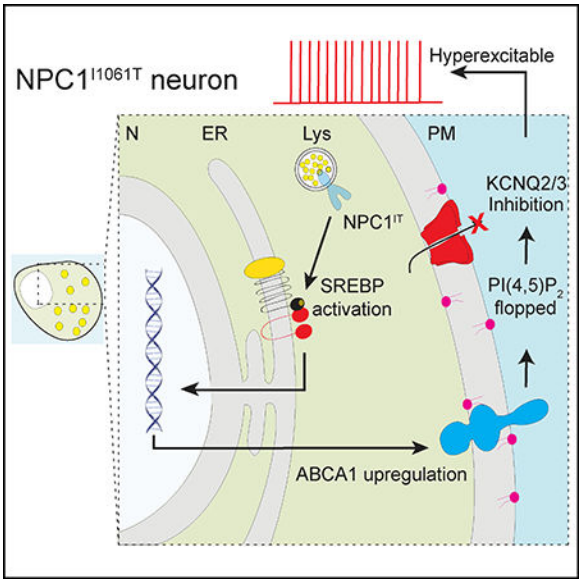

INTRODUCTION

Neurodegeneration is a common feature of many neurological disorders. Cell biological, genetic, and *in vivo* work increasingly emphasizes the crucial role that lysosomes play in neurodegeneration. Once simply thought of as acidic centers for degradation and recycling, lysosomes are now known to be highly dynamic signaling organelles that can mediate signal transduction via the mammalian target of rapamycin complex 1 (mTORC1) and regulate gene expression via transcription factor EB (TFEB) and other transcription factors (Laplante and Sabatini, 2012). These pathways are particularly relevant for maintaining brain homeostasis, as dysfunction of the endolysosomal and auto-phagic pathways has been associated with common neurodegenerative diseases, such as Alzheimer and Parkinson (Fraldi et al., 2016; Laplante and Sabatini, 2012), and lysosomal storage disorders—a group of inherited disorders characterized by the intralysosomal buildup of partially degraded metabolites, including cholesterol (Castellano et al., 2017; Schulze and Sandhoff, 2011).

Increasingly, dysregulation of cholesterol homeostasis is proposed as a contributing factor in the development of neurodegenerative disorders (Abdel-Khalik et al., 2017; Chang et al., 2017; Di Paolo and Kim, 2011; Eriksson et al., 2017). A main source of neuronal cholesterol is the internalization of cholesterol that is synthesized by glia. This import of cholesterol is predominantly mediated by astrocyte-derived apolipoprotein E (ApoE)-containing lipoprotein particles (Boyles et al., 1989; Herz and Bock, 2002). These lipoproteins are internalized via clathrin-mediated endocytosis and delivered to late lysosomal compartments where acidic lipases liberate cholesterol. The free cholesterol is transferred by the luminal

Niemann-Pick C2 protein to the membrane-bound Niemann-Pick type C1 (NPC1) protein for export to the endoplasmic reticulum (ER) by sterol transfer proteins (e.g., ORP5, ORPL1) at membrane contact sites between the ER and the lysosome (Du et al., 2011; Karten et al., 2009; Li et al., 2016; Luo et al., 2017; Zhao and Ridgway, 2017). The importance of the NPC1 protein in regulating the transfer of cholesterol to the ER is underscored by the severity of the fatal Niemann-Pick type C1 (NPC1) neurodegenerative disease. This autosomal recessive lysosomal storage disorder most commonly occurs due to a single I1061T substitution that results in misfolding of the NPC1 protein and subsequent targeting for ER-associated degradation (Gelsthorpe et al., 2008). The reduction in functional NPC1 protein results in massive luminal accumulation of cholesterol in lysosomes and cellular changes in cholesterol homeostasis (Millard et al., 2000). Neurologically, NPC1 patients typically exhibit progressive impairment of motor and intellectual function, before succumbing to the disease, tragically within the first 2 decades of life (Vanier, 1999). Despite the commonality of altered cholesterol metabolism and compromised neuronal function in neurodegenerative disorders, the molecular mechanisms that link cellular changes in cholesterol with alterations in neuronal excitability are absent. Thus, this monogenetic disease, with such profound alterations in cholesterol metabolism, allows us to test the hypothesis that altered lysosomal cholesterol metabolism can change the intrinsic electrical excitability of neurons (Figure 1A).

Neuronal excitability depends on the proper function of ion channels whose activities can be tuned by plasma membrane (PM) lipids, including cholesterol and the minor phosphoinositide, phosphatidylinositol 4,5-bisphosphate (PtdIns(4,5)P_2). PtdIns(4,5)P_2 regulates upward of 100 ion channels and transporters (Hilgemann et al., 2001; Hille et al., 2015), while cholesterol commonly suppresses the activity of several types of channels, including inwardly rectifying K^+ channels (Romanenko et al., 2004), Ca^{2+}-sensitive K^+ channels (Bukiya et al., 2011; Crowley et al., 2003; Purcell et al., 2011), and voltage-gated K^+ channels (Abi-Char et al., 2007; Hajdú et al., 2003). Despite separate biosynthetic pathways, the metabolism of cholesterol and phosphoinositides is not as distinct as previously thought. The transport of cholesterol between intracellular membranes at membrane contact sites uses phosphoinositides as the driving force to transport cholesterol (Mesmin et al., 2013). Another link between cholesterol and phosphoinositide metabolism involves the ABCA1 cholesterol transporter, which has been reported as being a PtdIns(4,5)P_2 floppase (exports PtdIns(4,5)P_2 out of the cell) (Gulshan et al., 2016). Hence, alterations in the cholesterol content of organelle membranes could dysregulate ion channel activity directly or indirectly by modifying PtdIns(4,5)P_2.

Here, we find that both pharmacological inhibition of NPC1 and its genetic mutation in an established transgenic animal model of the disease render neurons hyperexcitable. Furthermore, we discover that reduced KCNQ2/3 current density underlies this electrical hyperexcitability, which is mediated by a significant reduction in the abundance of PM PtdIns(4,5)P_2. The molecular mechanism that leads to a reduction in PtdIns(4,5)P_2 in NPC1 disease is a sterol regulatory element-binding protein (SREBP)-dependent upregulation of ABCA1. These data support the hypothesis that the regulated efflux of cholesterol from lysosomal membranes via NPC1 continually aids in the regulation of neuronal excitability

and reveals a link between lysosomal cholesterol and phosphoinositide metabolism in NPC1 disease. This link could have broad implications for other neurodegenerative disorders.

RESULTS

Pharmacological Inhibition of NPC1 Increases Neuronal Excitability

NPC1 disease cells exhibit a characteristic accumulation of cholesterol in lysosomes (Gelsthorpe et al., 2008; Millard et al., 2000; Yu et al., 2005). This cellular phenotype has become useful in the diagnosis of NPC1 disease since it is readily identifiable following staining with the naturally fluorescent polyene antibiotic, filipin (Vanier and Latour, 2015). Figure 1B presents confocal micrographs of filipin-stained fibroblasts isolated from healthy and NPC1 patients carrying the most prevalent mutation ($NPC1^{I1061T}$) (Millat et al., 1999; Park et al., 2003). Analysis of these images revealed that $NPC1^{I1061T}$ fibroblasts have larger cholesterol-containing vesicles (Figure 1C), with the median vesicle size of healthy fibroblasts being 0.22 μm^2 (Q1 = 0.13 μm^2 and Q3 = 0.39 μm^2) and $NPC1^{I1061T}$ fibroblasts being 0.38 μm^2 (Q1 = 0.18 μm^2 and Q3 = 0.75 μm^2). To mimic the cholesterol accumulation phenotype of NPC1 disease in isolated neurons, we used the well-characterized NPC1 inhibitor U18666A (U18; 1 μM). This cationic amphiphile directly binds to the sterol-sensing domain of the NPC1 protein (Lu et al., 2015) and blocks the efflux of cholesterol from lysosomes (Lange et al., 2000), thereby mimicking NPC1 disease. Cultured sympathetic (Figures 1D and 1E) or hippocampal (Figure S1A) neurons were treated overnight in the presence of U18 and stained with filipin. Similar to $NPC1^{I1061T}$ patient fibroblasts, U18 treatment induced the accumulation of cholesterol within vesicles (Figures 1D and 1E). While the median vesicle size of neurons cultured without U18 (control) was 0.03 μm^2 (Q1 = 0.01 μm^2 and Q3 = 0.12 μm^2), the median vesicle size of neurons cultured in the presence of U18 was 0.11 μm^2 (Q1 = 0.02 μm^2 and Q3 = 0.49 μm^2). Thus, treatment of neurons with U18 mimics the accumulation of cholesterol observed in fibroblasts from $NPC1^{I1061T}$ patients and represents a pharmacological tool to dissect the role of lysosome cholesterol efflux in regulating neuronal function.

To test whether U18-induced cholesterol accumulation alters neuronal excitability, action potentials (APs) were recorded in current-clamp mode using the perforated-patch configuration. Figure 1F shows recordings from a representative neuron cultured in the absence of U18 (control). Here, injecting 40 pA elicits a solitary AP despite the depolarizing stimulus being applied for 1 s (black trace). This typical firing pattern of sympathetic neurons corresponds to the cell adapting to the stimulus (spike adaptation) (Brown and Passmore, 2009; Zaika et al., 2006). In striking contrast, the same stimulus induced the firing of 9 APs in a neuron cultured in the presence of U18 (Figure 1F, U18, black trace). We interpreted this result as a loss of spike adaptation. From these data it is also noticeable that the neuron cultured in the presence of U18 fired more APs per unit of injected current (e.g., 20 pA, red trace) compared to the control neuron. To quantify changes in excitability, we measured the following: (1) the resting membrane potential (V_{rest}), (2) the amount of current injected necessary to elicit at least 1 AP (loosely called here rheobase), and (3) the number of APs fired with increasing current injections. Neurons cultured in the presence of U18 had a 9 mV more depolarized V_{rest} (Figure 1G, control: −59 ± 2 mV, U18: −50 ± 2 mV),

required less current injection to induce AP firing (Figure 1H, control: 37 ± 5 pA, U18: 17 ± 4 pA), and fired more APs per picoampere of current injected (Figure 1I). These U18-mediated alterations in AP firing could also be recapitulated in cultured hippocampal neurons (Figures S1B and S1C). In conclusion, inhibiting NPC1-mediated cholesterol egress from the lysosome leads to neurons becoming more excitable.

NPC1^{I1061T} Disease Neurons Are Hyperexcitable

Overnight application of U18 has been used extensively to investigate cellular changes in NPC1 disease. Despite its utility in doing so, this inhibition is acute relative to the chronic changes that occur during disease development in patients. Accordingly, the changes in electrical activity described above could represent transient changes in excitability observed when NPC1 is inhibited for hours; but over longer periods, neurons may adapt to restore their excitability. Therefore, to test whether neurons were also hyperexcitable in conditions closer to those of patients suffering from NPC1 disease (Figure 2A), we isolated neurons from a recently developed NPC1^{I1061T} knockin murine model (Praggastis et al., 2015). Figure 2B shows micrographs of filipin-stained neurons isolated from NPC1^{I1061T} mice compared to littermate WT controls. Similar to patient fibroblasts and U18-treated neurons, NPC1^{I1061T} neurons exhibit an enhanced accumulation of cholesterol within vesicular structures, with the distribution of vesicle size shifted toward larger vesicles in NPC1^{I1061T} neurons. While the median vesicle size in neurons from WT mice was 0.01 μm^2 (Q1 = 0.01 μm^2 and Q3 = 0.08 μm^2), the median vesicle size in neurons from NPC1^{I1061T} mice was 0.12 μm^2 (Q1 = 0.02 μm^2 and Q3 = 0.34 μm^2). Next, we measured AP firing in WT and NPC1^{I1061T} neurons. Figure 2D contrasts the electrical responses from representative neurons of each group. Comparable to what was observed following NPC1 inhibition, a 40-pA current injection induced the firing of a solitary AP in WT neurons, whereas the same injection stimulus produced 9 APs to fire from an NPC1^{I1061T} neuron. Analysis of neuronal electrical properties revealed that NPC1^{I1061T} neurons had an 8-mV more depolarized V_{rest} (Figure 2E, WT: −56 ± 1 mV, n = 20; NPC1^{I1061T}: −48 ± 2 mV), required less current to induce AP firing (Figure 2F, WT: 29 ± 4 pA; NPC1^{I1061T}: 14 ± 2 pA), and fired a greater number of APs per picoampere of current injected (Figure 2G, 100 pA; WT: 4 ± 1 AP; NPC1^{I1061T}: 16 ± 2 APs). These results show that the most prevalent NPC1 disease-causing mutation renders neurons hyperexcitable, suggesting a common mechanism that relates lysosomal cholesterol transport to the ability of neurons to send and receive electrical inputs.

Loss of NPC1 Function Reduces KCNQ2/3 Current ($I_{KCNQ2/3}$)

Based on the significant changes in neuronal firing behavior, we hypothesized that KCNQ2/3 voltage-gated potassium channel (K_V 7.2/7.3) current density may be altered in NPC1 disease (Figure 3A). Our rationale follows: (1) KCNQ2/3 channels activate at negative potentials (~−65 mV) and thus help establish V_{rest}, (2) KCNQ2/3 channels open in response to depolarization to repolarize the membrane potential, and (3) KCNQ2/3 channels participate in spike frequency adaptation (Brown and Passmore, 2009). Thus, reduced $I_{KCNQ2/3}$ is expected to depolarize V_{rest} increase intrinsic electrical excitability, and decrease spike frequency adaption—all electrophysiological consequences observed in NPC1 disease neurons. Consequently, we measured $I_{KCNQ2/3}$ densities from U18-treated, NPC1^{I1061T}, and NPC1$^{-/-}$ neurons. $I_{KCNQ2/3}$ density was smaller following the inhibition of NPC1 (Figures

3B and 3C, 1.8 ± 0.3 pA/pF) compared to control neurons (5.9 ± 0.8 pA/pF). This reduction in $I_{KCNQ2/3}$ density was not observed following a 2-min acute application of the inhibitor, ruling out a direct inhibition or block of the channel (Figure S2). Furthermore, $I_{KCNQ2/3}$ density was also smaller in neurons from $NPC1^{I1061T}$ mice (Figures 3D and 3E, WT: 9.0 ± 1.0 pA/pF; $NPC1^{I1061T}$: 4.2 ± 0.8 pA/pF) and $NPC1^{-/-}$ mice (Figures 3F and 3G, WT: 6.8 ± 0.8 pA/pF; $NPC1^{-/-}$: 2.9 ± 0.4 pA/pF). Consequently, inhibition, deletion, or disease-causing mutation of the NPC1 cholesterol transporter reduce $I_{KCNQ2/3}$ density and offer a potential mechanism underlying the hyperexcitability phenotype in NPC1 disease.

Opening KCNQ2/3 Channels Rescues $NPC1^{I1061T}$ Neuron Excitability

Following the premise that the reduction of $I_{KCNQ2/3}$ leads to a hyperexcited state in neurons with non-functional NPC1, we predicted that the application of retigabine, a KCNQ2/3 channel opener (Gunthorpe et al., 2012), would make them less excitable (Figure 4A). Bath application of 10 mM retigabine quickly and reversibly restored the normal firing behavior of U18-treated neurons (Figures 4B–4E), with fewer APs recorded per picoampere of current injected (100 pA; U18 treated: 19 ± 1 AP; with retigabine: 3 ± 2 APs; washout: 18 ± 1 APs; n = 8, $p < 0.0001$ for U18 versus retigabine; $p = 0.5$ for U18 versus washout; and $p < 0.0001$ for retigabine versus washout). Retigabine was also effective at abrogating the hyperexcited state of $NPC1^{I1061T}$ neurons (Figure 4F, 100 pA; $NPC1^{I1061T}$: 16 ± 2 APs; $NPC1^{I1061T}$ + retigabine: 8 ± 3). These results support the hypothesis that a reduction in $I_{KCNQ2/3}$ density is responsible for the enhanced excitability observed in NPC1 disease neurons.

PM PtdIns(4,5)P_2 Is Reduced in NPC1 Disease

We next asked what mechanism underlies the reduction in $I_{KCNQ2/3}$. First, we ruled out the possibility that KCNQ channel abundance was altered in NPC1 disease (Figure S3). Then, we tested the hypothesis that PtdIns(4,5)P_2 is altered in NPC1 disease. PtdIns(4,5)P_2 is the most abundant phosphoinositide at the PM and is absolutely required for KCNQ2/3 channel function (Suh and Hille, 2002; Zhang et al., 2003); hence, any reductions in PtdIns(4,5)P_2 could lead to reduced $I_{KCNQ2/3}$ (Figure 5A). To determine whether PtdIns(4,5)P_2 is altered in NPC1 disease, we took two approaches: expression of a fluorescently tagged, genetically encoded PtdIns(4,5)P_2 biosensor (yellow fluorescent protein [YFP]-pleckstrin homology domain $[PH]_{PLC\delta1}$) and ultrahigh pressure liquid chromatography coupled to tandem mass spectrometry (UPLC-MS/MS). We chose these two complementary approaches because UPLC-MS/MS is extremely quantitative but does not distinguish specific PtdInsP_2 regioisomers (i.e., PtdIns(3,5)P_2 versus PtdIns(4,5)P_2), whereas the imaging approach is semiquantitative but offers spatial information and is excellent at differentiating specific regioisomers. Analysis of healthy and $NPC1^{I1061T}$ patient fibroblasts transfected with YFP-$PH_{PLC\delta1}$ revealed a decrease in the ratio of fluorescence intensity at the PM compared to the cytoplasm (Cyt) in $NPC1^{I1061T}$ patient fibroblasts (Figures 5B and 5C; WT: 4.0 ± 0.2, n = 21; $NPC1^{I1061T}$: 2.8 ± 0.2). In addition, MS showed a 50% reduction in total PtdInsP_2 in $NPC1^{I1061T}$ fibroblasts (Figure 5D; WT: $2.3 \times 10^6 \pm 0.6 \times 10^5$; $NPC1^{I1061T}$: $1.2 \times 10^6 \pm 0.8 \times 10^5$). To further test this hypothesis, we also measured PtdInsP_2 levels from three different brain regions (hippocampus, cortex, and cerebellum) of $NPC1^{I1061T}$ mice and found similar reductions in PtdInsP_2 across each region (Figures 5E–5H), with total PtdInsP_2 reduced by

66% (Figure 5I; WT = $6.6 \times 10^7 \pm 0.9 \times 10^7$; $NPC1^{I1061T} = 2.5 \times 10^7 \pm 0.7 \times 10^7$). These results indicate that PtdIns(4,5)P_2 is reduced in NPC1 disease and offers an underlying mechanism for the reduction of $I_{KCNQ2/3}$ and neuron hyperexcitability.

Exogenous Application of PtdIns(4,5)P_2 Rescues Both $I_{KCNQ2/3}$ and Excitability

Following the premise that neurons lacking functional NPC1 have less PtdIns(4,5)P_2 and consequently reduced $I_{KCNQ2/3}$ and increased excitability, we next asked whether exogenous dialysis of PtdIns(4,5)P_2 would increase $I_{KCNQ2/3}$ and rescue excitability in U18-treated neurons (Figure 6A). Patch-clamp electrophysiology was performed in whole-cell mode with pipettes filled with a standard internal solution or a solution supplemented with 30 μM diC8-PtdIns(4,5)P_2. Figure 6B shows representative recordings of $I_{KCNQ2/3}$ from control neurons patched with or without diC8-PtdIns(4,5)P_2. The addition of diC8-PtdIns(4,5)P_2 to the cell through the patch pipette did not change the current density in control neurons (Figure 6D, without diC8-PtdIns(4,5)P_2: 10.9 ± 2.0 pA/pF; with diC8-PtdIns(4,5)P_2: 7.8 ± 1.5 pA/pF). However, the addition of diC8-PtdIns(4,5)P_2 significantly increased $I_{KCNQ2/3}$ density in neurons cultured in the presence of U18 (8.4 ± 1.3 pA/pF) compared to neurons cultured in the presence of U18 alone (2.4 ± 0.9 pA/pF; Figures 6C and 6D). $I_{KCNQ2/3}$ density was not statistically different between control neurons and U18-treated neurons following the application of diC8-PtdIns(4,5)P_2, suggesting that the exogenous addition of PtdIns(4,5)P_2 rescues $I_{KCNQ2/3}$ in neurons lacking functional NPC1. Finally, we tested whether the addition of 30 μM diC8-PtdIns(4,5)P_2 rescues the excitability of neurons with inhibited NPC1. Figure 6E shows representative current-clamp recordings of U18 neurons treated with or without diC8PtdIns(4,5)P_2. Note that the addition of diC8-PtdIns(4,5)P_2 to neurons caused fewer APs to fire following a 40 pA current injection (1 AP, black trace) compared to a neuron cultured in the presence of U18 but patched without diC8-PtdIns(4,5)P_2 (9 APs, black trace). In fact, neurons patched with diC8PtdIns(4,5)P_2 fired fewer APs with every current injection tested, reaching a maximum of 5 ± 2 APs when neurons were stimulated with 100 pA current injection (n = 8), compared to 13 ± 3 APs when neurons were patched without PtdIns(4,5)P_2 (Figure 6F). In conclusion, exogenous application of diC8-PtdIns(4,5)P_2 to neurons lacking functional NPC1 is enough to rescue the hyperexcitable phenotype, supporting the hypothesis that these neurons have less PtdIns(4,5)P_2 and that the reduction of this lipid is the underlying mechanism of hyperexcitability in NPC1 disease.

Upregulation of ABCA1 Reduces PtdIns(4,5)P_2, Leading to Hyperexcitability in NPC1 Disease

Finally, we sought to determine the molecular link between the accumulation of cholesterol in the lysosome and the reduction of PtdIns(4,5)P_2 at the PM. A striking consequence of disrupting NPC1-dependent cholesterol efflux is the activation of SREBP, a transcription factor that controls the synthesis of cholesterol and other membrane lipids (Brown and Goldstein, 1997). This transcription factor not only controls cholesterol synthesis through an end product feedback mechanism but it also controls many other physiological processes. For instance, the overexpression of SREBP in myocytes changes the expression of ~1,500 genes (Rome et al., 2008). Considering the significant number of protein-coding genes under the control of SREBP, we tested whether crucial enzymes related to PtdIns(4,5)P_2

metabolism are altered in NPC1 disease (Figure 7A). To begin, we verified that the activation of SREBP, independent of NPC1 function, reduced PM PtdIns(4,5)P_2 (Figure S4). Next, determination of the protein abundances of PIP5K1A (phosphatidylinositol 4-phosphate 5-kinase type 1A), SYNJ1 (Synaptojanin 1), and PLC$_{\beta 1}$ (phospholipase C β1) revealed no significant difference between healthy and NPC1^{I1061T} (Figures 7B and 7C). Therefore, we ruled out the misregulation of any of these three important proteins as a possible mechanism for the reduction of PtdIns(4,5)P_2 in NPC1 disease.

Given that phosphoinositide lipid kinases or lipid phosphatases do not appear to underlie the reduction in PM PtdIns(4,5)P_2, we focused our attention on proteins that are key regulators of the transport of both cholesterol and phosphoinositide metabolism. To this end, we tested whether several known phosphoinositide transfer proteins (ORP2, ORPL1, ORP5/8) or the ABCA1 (ATP-binding cassette transporter-A1) transporter are differentially expressed in NPC1 disease. Oxysterol-binding protein (OSBP)-related proteins are transfer proteins that transfer cholesterol at membrane contact sites through the counter-transport of PtdIns4P and PtdIns(4,5)P_2 (Ghai et al., 2017; Mesmin et al., 2013; Wang et al., 2019; Zhao and Ridgway, 2017), whereas ABCA1 (ATP-binding cassette transporter-A1) is a transmembrane protein, which plays a major role in lipid homeostasis by regulating cholesterol efflux from the cell. In addition, ABCA1 has been recently reported to exhibit PtdIns(4,5)P_2 floppase activity, moving PtdIns(4,5)P_2 from the inner leaflet to the outer leaflet of the PM to mediate Apo1-dependent binding during nascent high-density lipoprotein (HDL) assembly (Gulshan et al., 2016). Determination of protein abundances revealed that the average fold change of ORP2 was 1.35 ± 0.05 (n = 3, p = 0.0004), ORPL1 was 1.33 ± 0.06 (n = 4, p = 0.002), ORP8 was 1.16 ± 0.25 (n = 4, p = 0.5), and ABCA1 was 3.3 ± 0.3 (n = 4, p = 0.002) in NPC1^{I1061T} fibroblasts (Figures 7I and S5). Thus, in NPC1 disease, several key phosphoinositide transfer proteins are differentially expressed. The fold change of OPR2 and ORPL1 is small compared to the >3-fold increase in ABCA1 abundance; therefore, we focused our attention on determining whether ABCA1 is responsible for reducing PtdIns(4,5)P_2, PtdIns(4,5)P_2-dependent ion channel current, and excitability in NPC1 disease.

To test for the involvement of ABCA1 in altering PtdIns(4,5)P_2, we took two complementary approaches that, independently of NPC1 function, increase the abundance of ABCA1. First, we treated healthy patient fibroblasts or neurons with an agonist of the nuclear liver factor receptor (LXR) T0901317 (Figures 7E, 7F, and S6), which upregulates the expression of ABCA1. Second, we used a cell line that stably expresses the ABCA1 transporter at a high copy number (Figures 7G and 7H). Under both experimental conditions, there was a lower PM-to-Cyt fluorescence intensity ratio of the PtdIns(4,5)P_2 biosensor (PH$_{PLC\delta 1}$), suggesting reduced PtdIns(4,5)P_2. Next, we tested the hypothesis that blocking ABCA1 rescues both $I_{KCNQ2/3}$ and excitability in NPC1 disease (Figure 7J). To block ABCA1, we added 10 μM probucol to neurons that were isolated from NPC1^{I1061T} mice. Blocking ABCA1 increased $I_{KCNQ2/3}$ density in NPC1^{I1061T} neurons from 1.8 ± 0.5 to 6.4 ± 1.1 pA/pF (Figure 7K, p = 0.005). Moreover, neurons from NPC1^{I1061T} mice treated with probucol fired 6.5 ± 1.7 APs with 100 pA current injection and exhibited more spike adaptation (Figure 7L, n = 9), meaning that they were less excitable than neurons from NPC1^{I1061T} mice (compare data from Figure 2G). Finally, treating U18 neurons with small interfering RNA (siRNA) directed against ABCA1 increased $I_{KCNQ2/3}$ current density,

restored the resting membrane potential, and rescued excitability (Figure S7). These data suggest that the loss of NPC1 function indirectly alters the level of proteins that transport both cholesterol and PtdIns(4,5)P_2, leading to decreased PM PtdIns(4,5)P_2, decreased $I_{KCNQ2/3}$, and, consequently, enhanced excitability.

DISCUSSION

Here, we show for the first time that both inhibition and disease-causing mutation of the lysosomal cholesterol transporter, NPC1, render neurons hyperexcitable, in that neurons have a more depolarized V_{rest}, less current is required to induce them to fire APs, and they lose the ability to complete spike adaptation. Changes in excitability result from reduced PM PtdIns(4,5)P_2 and the subsequent reduction of KCNQ2/3 channel function. Furthermore, the molecular mechanism that links cholesterol accumulation and PtdIns(4,5)P_2 reduction is the upregulation of ABCA1. Based on these data, we propose that NPC1 disease is a phosphoinositide-deficient disease and that ABCA1 links lysosomal cholesterol efflux with PM phosphoinositide levels to tune neuronal excitability.

PtdIns(4,5)P_2 Deficiency Underlies Neuronal Hyperexcitability in NPC1 Disease

Like many monogenetic disorders, despite the seemingly nondescript nature of a single mutation, the mechanisms of NPC1 pathogenesis are complicated. For NPC1 disease, >1,500 genes (Rome et al., 2008) and ~300 proteins (Rauniyar et al., 2015) are differentially regulated. At the cellular level, these alterations manifest as defects in vesicular trafficking, mTOR signaling (Castellano et al., 2017), lysosomal calcium handling (Lloyd-Evans et al., 2008), and lipid localization (Lloyd-Evans et al., 2008; Praggastis et al., 2015). We report for the first time hyperexcitability in NPC1 disease. Evidence presented in this study suggests that the mechanism underlying this enhanced excitability is a reduction in $I_{KCNQ2/3}$ mediated by a decline in PtdIns(4,5)P_2. Could other lipids altered in NPC1 disease, such as cholesterol or sphingolipids, account for the reduction in $I_{KCNQ2/3}$? For cholesterol, KCNQ2/3 channels are reported as being negatively regulated by PM cholesterol (Lee et al., 2010). In cells lacking functional NPC1, there is a described reduction in the amount of cholesterol in the endofacial leaflet of the PM (Maekawa and Fairn, 2015). Thus, decreased PM cholesterol in NPC1 disease would disinhibit KCNQ2/3 channels and result in more current, which is the opposite of our observations. Another lipid that accumulates in lysosomes in NPC1 disease is sphingosine-1-phosphate (S1P) (Praggastis et al., 2015). Some reports show that KCNQ2/3 channel activity can be weakly stimulated (increase in channel open probability [P_o] to 0.16) by a high concentration (100 μM) of S1P (Telezhkin et al., 2012). In contrast, a lower concentration (10 μM) of PtdIns(4,5)P_2 is enough to activate KCNQ2/3 channels with a P_o of 0.54. Therefore, if S1P is reduced in the PM of NPC1 disease neurons, it would be anticipated that the differences in affinity that KCNQ2/3 has for each lipid would mean that any S1P effects would be secondary to PtdIns(4,5)P_2-dependent alterations. In conclusion, decreases in either cholesterol or S1P appear unlikely to account for the reductions of $I_{KCNQ2/3}$ in NPC1 disease.

Cholesterol and PtdIns(4,5)P_2 Dysregulation in Neurodegenerative Diseases

We present evidence linking the disruption of lysosomal cholesterol efflux with decreases in PtdIns(4,5)P_2-dependent KCNQ2/3 channel activity, leading to aberrant neuronal activity. At the molecular level, our data suggest that the cholesterol transporter and PtdIns(4,5)P_2 floppase, ABCA1, is responsible for the decline in PtdIns(4,5)P_2 that consequently modifies the electrical properties of NPC1 disease neurons. Fibroblasts from patients with Tangier disease, a disease caused by mutations in ABCA1, transfer 50% less PtdIns than fibroblasts from healthy patients (von Eckardstein et al., 1998), while mutations in ABCA1 have been associated with a higher risk of Alzheimer disease (Nordestgaard et al., 2015). Thus, there is a precedent for the involvement of ABCA1 as a potential contributing factor in neurodegeneration. Is there evidence in the literature to suggest that other neurodegenerative diseases have either dysfunction of KCNQ2/3 channel activity or altered levels of PtdIns(4,5)P_2? In fact, there is accumulating evidence that mutations in the genes encoding KCNQ2/3 subunits or PtdIns(4,5)P_2-metabolizing enzymes lead to neuropathies similar to those in NPC1 disease. Mutations in KCNQ2/3 cause the hyperexcitability of neurons, leading to epileptic phenotypes in neonatal epilepsy (Jentsch, 2000; Watanabe et al., 2000), Huntington disease (Cao et al., 2015), and the bulbar form of amyotrophic lateral sclerosis (ALS) (Ghezzi et al., 2018). Opening KCNQ2/3 channels with retigabine protects motoneurons against the excitotoxicity characteristic of this form of ALS (Ghezzi et al., 2018). Further, mutations in the enzymes responsible for PtdIns(4,5)P_2 synthesis are associated with Alzheimer disease (Zhu et al., 2015), Parkinson disease (Cao et al., 2017), and Friedreich ataxia (Bayot et al., 2013), another rare neurodegenerative disease. These data support the idea that maintaining PtdIns(4,5)P_2 levels in neurons is essential for normal brain function and that dysfunction of KCNQ2/3 channel activity may be a contributing factor to the progression of neurodegenerative diseases. It is important to note that the relationship between enhanced neuronal excitability and neurodegeneration in NPC1 disease is correlative at this point. Given the fundamental importance of regulated ion channel function and Ca^{2+} homeostasis for neuron health and the Ca^{2+} hypothesis of neurodegeneration, which posits that altered Ca^{2+} dynamics contribute to neuropathology (Berridge, 2010), we hypothesize that alterations in the excitability alluded to above would facilitate enhanced Ca^{2+} influx into cerebellar neurons, potentially leading to their degeneration in NPC1 disease. Future experiments are needed to establish causation between hyperexcitability and cell death in NPC1 disease.

To conclude, mutations within the NPC1 protein lead to a poorly understood sequence of events that end in neurodegeneration and premature death. We have defined steps in the pathogenic cascade of NPC1 disease, namely upregulation of ABCA1 leading to a decrease in PM PtdIns(4,5)P_2 and $I_{KCNQ2/3}$, which produces hyperexcitability in neurons. Thus, NPC1 disease is not only a cholesterol storage disease but also a phosphoinositide-deficient disorder with a hyperexcitability phenotype.

STAR⋆METHODS

Detailed methods are provided in the online version of this paper and include the following:

CONTACT FOR REAGENT AND RESOURCE SHARING

Further information and requests for resources and reagents should be directed to and will be fulfilled by the Lead Contact, Eamonn J. Dickson (ejdickson@ucdavis.edu).

EXPERIMENTAL MODEL AND SUBJECT DETAILS

Murine models of NPC1 disease—NPC1 knock-out ($NPC^{-/-}$, RRID: IMSR_JAX: 003092), $NPC1^{I1061T}$ knock-in (Praggastis et al., 2015), and wild-type (WT) mice from a C57BL/6 background were kindly provided by Daniel Ory (Washington University Saint Louis). Male C57BL/6 WT mice used for experiments involving U18666A (U18, SIGMA, Cat # 662015) were purchased from the Jackson Laboratory (RRID: IMSR_JAX:000664). All animals were kept in an animal facility with controlled conditions and were given standard chow and water *ad libitum*. The animal handling protocol was approved by the University of California Institutional Animal Care and Use Committee. To genotype $NPC1^{I1061T}$ mice, we extracted DNA and amplified an NPC1 allele with the following primers: forward (5′-tgatctgcacacttggaaccgag-3′) and reverse (5′-cactgccttgagcagcatctcag-3′). WT allele was identified by a 200 bp fragment, whereas the knock-in allele was identified by a 234 bp fragment. Heterozygous mice, containing both 200 bp and 234 bp, were not used in this study. Experiments using either knock-out or knock-in animals were conducted using both males and females. Knock-out animals were used at around 70 days old. Knock-in animals were used at around 90 days old.

Cell lines—Fibroblast cell lines from a healthy male (GM05659, RRID: CVCL_7434) and a male patient with a homozygous mutation in $NPC1^{I1061T}$ (GM18453, RRID: CVCL_DA78, from the NIGMS repository) were purchased from the Coriell Institute. Fibroblasts were grown in Eagle's Minimum Essential Medium (MEM) with Earle's salts and non-essential amino acids (SIGMA, Cat # M5650) supplemented with 2 mM L-glutamine (GIBCO, Cat # 25030–081), 15% non-inactivated fetal bovine serum (GIBCO, Cat # 26140–079) and 0.2% penicillin/streptomycin (GIBCO, Cat # 15140–122), passaged twice a week, and incubated in 5% CO_2 at 37°C.

HeLa cells stably expressing ABCA1-GFP were provided by Dr. Alan Remaley, NHLBI, Bethesda, MD. HeLa cells were grown in DMEM (GIBCO, Cat # 11995–065) supplemented with 10% non-inactivated fetal bovine serum and 0.2% penicillin/streptomycin, passaged twice a week, and incubated in 5% CO2 at 37°C. Expression of ABCA1-GFP HeLa cells was induced by adding 150 μg/ml geneticin (GIBCO, Cat # 10131–035) and 200 μg/ml Hygromycin (Invitrogen, Cat # 10687010).

METHOD DETAILS

Neuron isolation—Neurons from superior cervical ganglion (SCG) were prepared from 10 to 16 week-old female or male mice by enzymatic digestion following a standardized protocol for rats (Vivas et al., 2013) but reducing the amount of enzymes. Briefly, mice were anesthetized with pentobarbital sodium (VETONE, Cat # 501016) before extraction of the SCG. SCG were cleaned and sliced into 4 pieces. This tissue was transferred to a tube containing 10 U/ml papain (SIGMA, Cat # 4762) in Hank's solution and kept at 37°C for 6 min, then it was transferred to a solution containing 0.33 mg/ml collagenase type II

(Worthington, Cat # LS004176) and 2.5 mg/ml dispase (GIBCO, Cat # 0479) for up to 60 min. Every 20 min the tissue was pipetted to dissociated into individual cells. After obtaining a homogeneous cell suspension, cells were washed with DMEM followed by centrifugation at 180 g for 3 min. Washing step was repeated 3 times. Isolated neurons were plated on poly-L-lysine (MW > 300,000, SIGMA, Cat # P5899) coated glass coverslips and incubated in 5% CO_2 at 37°C in DMEM supplemented with 10% FBS and 0.2% penicillin/streptomycin. Neurons were used up to 24 h after plating.

Filipin Staining and Super-resolution Imaging—Cells washed with PBS were fixed with a mix of 3% paraformaldehyde (Electron Microscopy Sciences, Cat # 15710) and 0.1% glutaraldehyde (SIGMA, Cat # G7651) for 10 min at 21°C. Following a 5-minute incubation with sodium borohydrate (10 mM, SIGMA, Cat #, 213462), cells were stained with 3 mg/ml filipin (SIGMA, Cat # F9765) for 2 h at room temperature. Cells were imaged in PBS. During the filipin staining process cells were protected from unnecessary light exposure. Cells were imaged using a Zeiss880 AiryScan microscope (axial resolution of 120 nm) by exciting with a 405 nm LED. This imaging mode allowed us to resolve cholesterol-containing vesicles.

Electrophysiological Recordings—All electrophysiological recordings were performed at room temperature. Voltage responses were recorded using perforated-patch configuration (except Figure 6) in the current-clamp mode, whereas KCNQ2/3 current was recorded using the whole-cell configuration in voltage clamp mode. To isolate KCNQ2/3 tail currents, the voltage was held at −20 mV, before stepping to −60 mV. The amplitude of KCNQ2/3 currents was measured from the resulting currents relative to the current at the end of the pulse (current close to 0 pA). We used an Axopatch 200B amplifier coupled with an Axon Digidata 1550B data acquisition board (Molecular Devices Electrophysiology) to acquire the electrical signals. Patch pipettes had a resistance of 2 – 6 MΩ. Liquid junction potential of 4 mV was calculated using the pCLAMP 10 software and was not corrected for, hence the V_{rest} reported in the Results section is in fact 4 mV more negative (around −63 mV in WT SCG neurons). Voltage responses were sampled at 5 KHz, whereas currents were sampled at 2 KHz. For current recordings, cell capacitance was cancelled out and series resistances of < 10 MΩ were compensated by 60%. Due to remaining series resistance, voltage error is expected to be < 4 mV. The bath solution (Ringer's solution) contained 150 mM NaCl, 2.5 mM KCl, 2 mM $CaCl_2$, 1 mM $MgCl_2$, 10 mM HEPES, and 8 mM glucose, adjusted to pH 7.4 with NaOH. The internal solution used to fill the patch pipettes contained 175 mM KCl, 1 mM $MgCl_2$, 5 mM HEPES, 0.1 mM K_4BAPTA, 3 mM Na_2ATP, and 0.1 mM Na_3GTP, adjusted to pH 7.2 with KOH. For current-clamp recordings, 30 μM amphotericin B (SIGMA, Cat # A4888) was added to the internal solution to facilitate electrical access to the cell. The bath solution was perfused at 2 ml/minute, permitting solution exchange surrounding the recording cell with a time constant of 4 s. DiC8-PtdIns(4,5)P_2 (30 μM, Avanti Polar Lipids, Cat # 850185) was added in the internal solution.

Protein extraction and abundance determination—Protein from cell cultures, SCG, or brain tissue was harvested in RIPA buffer (Thermo Scientific, Cat # 89900) with Complete, Mini, EDTA-free protease inhibitor cocktail (Roche, Cat # 11836170001) for 15

min at 4°C. For SCG and brain tissue, protein samples were sonicated using a bath sonicator at 4°C. Postnuclear supernatant was isolated by centrifuging for 20 minutes at 13,600 g at 4°C. Protein concentration was quantified with a plate reader using the Pierce BCA protein assay kit (Thermo Scientific, Cat # 23225). Protein samples were resolved in 4%–12% Bis-Tris gels under reducing conditions. Proteins were transferred onto nitrocellulose membranes (Life Technologies, Cat # LC2000) using the Mini-Bolt system (Thermo Scientific, Cat # A25977). Membranes were blotted using rabbit monoclonal anti-NPC1 (Abcam, Cat # ab134113, RRID: AB_2734695, 1:1,000), rabbit anti-KCNQ2 (Abcam, Cat # ab22897, RRID: AB_775890, 1:500), mouse anti-ABCA1 (Abcam, Cat # ab18180, RRID: AB_444302, 1:1000), rabbit anti-PIP5K1A (Cell Signaling Technology, Cat # 9693, RRID: AB_2164698, 1:500), rabbit anti-SYNJ1 (SIGMA, Cat # HPA011916, RRID: AB_1857692, 1:500), rabbit anti-$PLC_{\beta 1}$ (Abcam, Cat # ab182359, 1:1000), and mouse anti-β-actin (Thermo Scientific, Cat # MA1–91399, RRID: AB_2273656, 1:10,000). Blotted bands were detected using fluorescent secondary antibodies goat anti-rabbit 680RD (P/N 926–68071, LI_COR biosciences, RRID: AB_10956389, 1:10,000) and goat anti-mouse 800CW (P/N 925–32210, LI_COR biosciences, RRID: AB_2687825, 1:20,000). ImageJ was used to calculate fluorescence density of each band. The abundance of NPC1 or KCNQ2 from $NPC1^{I1061T}$ or U18-treated tissue was reported as normalized to β-actin and relative to the abundance in WT or control tissue.

Measuring PtdIns(4,5)P_2—To measure PtdIns(4,5)P_2 in fibroblasts, a plasmid for $PH_{PLC\delta 1}$ tagged with YFP was transfected (0.2 μg DNA) using Lipofectamine LTX (Invitrogen, Cat # 11668–027). Imaging of this biosensor was performed 24 h post-transfection using a spinning disk confocal microscope (Andor W-1 spinning disk). To measure PtdIns(4,5)P_2 from fibroblasts and brain samples by mass spectrometry, lipids were extracted with butanol and chloroform, as described previously (Traynor-Kaplan et al., 2017). A PtdIns(4,5)P_2 standard was added 17:0, 20:4 PtdIns(4,5)P_2 (Avanti Lipids, Cat # LM-1904) to all biological samples. Samples were neutralized by methylation and infused with sodium formate and analyzed using a Waters XEVO TQ-S MS/MS in multiple reaction monitoring mode (MRM) using electrospray and positive ion mode. Elution profiles plotting the intensity (arbitrary units) as a function of elution time (minutes) were analyzed to determine relative changes in PtdInsP_2 levels between samples. Total integrated areas under peaks from samples and standards were quantified using MassLynx software (Waters, RRID: SCR_014271). Peak areas of PIP_2 from the biological sample were normalized to the synthetic standard and further corrected for tissue amount using total protein.

QUANTIFICATION AND STATISTICAL ANALYSIS

We used IGOR Pro (IGOR Software, WaveMetrics, RRID: SCR_000325), Excel (Microsoft), and Prism (GraphPad, RRID: SCR_002798) to analyze data. ImageJ (RRID: SCR_003070) was used to process images. Data were collected from independent experiments from at least three mice and are presented as Mean ± SEM. For the super-resolution data of vesicle size, the median, first (Q1), and third (Q3) quartiles instead of the mean was used given that the data were not normally distributed (Normality test in Prism). A non-parametric statistical test (Mann-Whitney Wilcoxon) was used to test for statistical significance between vesicle size in different conditions. All other statistical analyses

presented in this study were performed using parametric Student's t test, considering p values < 0.05 as statistical significance. The number of cells used for each experiment is detailed in each figure legend.

Supplementary Material

Refer to Web version on PubMed Central for supplementary material.

ACKNOWLEDGMENTS

We thank Drs. Fernando Santana, Manuel Navedo, and Claudia Moreno and members of the Dickson and Dixon laboratories for helpful comments and discussions on the manuscript; Dale Whittington, Dr. Alexis Traynor-Kaplan, and the other members of the Washington University School of Pharmacy Mass Spectrometry Center for help and advice, and Elizabeth Quasebarth for help and guidance on the $NPC1^{I1061T}$ animal model. This work was supported by R01GM127513 and University of California funds (to E.J.D.), Pharmacology T32 training award T32GM099608 (to S.A.T.), AHA grant 15SDG25560035 (to R.E.D.), and NIH R01HL06773 (to D.S.O.).

REFERENCES

Abdel-Khalik J, Yutuc E, Crick PJ, Gustafsson J-Å, Warner M, Roman G, Talbot K, Gray E, Griffiths WJ, Turner MR, and Wang Y (2017). Defective cholesterol metabolism in amyotrophic lateral sclerosis. J. Lipid Res 58, 267–278. [PubMed: 27811233]

Abi-Char J, Maguy A, Coulombe A, Balse E, Ratajczak P, Samuel JL, Nattel S, and Hatem SN (2007). Membrane cholesterol modulates Kv1.5 potassium channel distribution and function in rat cardiomyocytes. J. Physiol 582, 1205–1217. [PubMed: 17525113]

Bayot A, Reichman S, Lebon S, Csaba Z, Aubry L, Sterkers G, Husson I, Rak M, and Rustin P (2013). Cis-silencing of PIP5K1B evidenced in Friedreich's ataxia patient cells results in cytoskeleton anomalies. Hum. Mol. Genet 22, 2894–2904. [PubMed: 23552101]

Berridge MJ (2010). Calcium hypothesis of Alzheimer's disease. Pflugers Arch. 459, 441–449. [PubMed: 19795132]

Boyles JK, Zoellner CD, Anderson LJ, Kosik LM, Pitas RE, Weisgraber KH, Hui DY, Mahley RW, Gebicke-Haerter PJ, Ignatius MJ, et al. (1989). A role for apolipoprotein E, apolipoprotein A-I, and low density lipoprotein receptors in cholesterol transport during regeneration and remyelination of the rat sciatic nerve. J. Clin. Invest 83, 1015–1031. [PubMed: 2493483]

Brown MS, and Goldstein JL (1997). The SREBP pathway: regulation of cholesterol metabolism by proteolysis of a membrane-bound transcription factor. Cell 89, 331–340. [PubMed: 9150132]

Brown DA, and Passmore GM (2009). Neural KCNQ (Kv7) channels. Br. J. Pharmacol 156, 1185–1195. [PubMed: 19298256]

Bukiya AN, Belani JD, Rychnovsky S, and Dopico AM (2011). Specificity of cholesterol and analogs to modulate BK channels points to direct sterol-channel protein interactions. J. Gen. Physiol 137, 93–110. [PubMed: 21149543]

Cao Y, Bartolomé-Martín D, Rotem N, Rozas C, Dellal SS, Chacon MA, Kadriu B, Gulinello M, Khodakhah K, and Faber DS (2015). Rescue of homeostatic regulation of striatal excitability and locomotor activity in a mouse model of Huntington's disease. Proc. Natl. Acad. Sci. USA 112, 2239–2244. [PubMed: 25646456]

Cao M, Wu Y, Ashrafi G, McCartney AJ, Wheeler H, Bushong EA, Boassa D, Ellisman MH, Ryan TA, and De Camilli P (2017). Parkinson Sac Domain Mutation in Synaptojanin 1 Impairs Clathrin Uncoating at Synapses and Triggers Dystrophic Changes in Dopaminergic Axons. Neuron 93, 882–896.e5. [PubMed: 28231468]

Castellano BM, Thelen AM, Moldavski O, Feltes M, van der Welle REN, Mydock-McGrane L, Jiang X, van Eijkeren RJ, Davis OB, Louie SM, et al. (2017). Lysosomal cholesterol activates mTORC1 via an SLC38A9-Niemann-Pick C1 signaling complex. Science 355, 1306–1311. [PubMed: 28336668]

Chang TY, Yamauchi Y, Hasan MT, and Chang C (2017). Cellular cholesterol homeostasis and Alzheimer's disease. J. Lipid Res 58, 2239–2254. [PubMed: 28298292]

Crowley JJ, Treistman SN, and Dopico AM (2003). Cholesterol antagonizes ethanol potentiation of human brain BKCa channels reconstituted into phospholipid bilayers. Mol. Pharmacol 64, 365–372. [PubMed: 12869641]

Di Paolo G, and Kim TW (2011). Linking lipids to Alzheimer's disease: cholesterol and beyond. Nat. Rev. Neurosci 12, 284–296. [PubMed: 21448224]

Du X, Kumar J, Ferguson C, Schulz TA, Ong YS, Hong W, Prinz WA, Parton RG, Brown AJ, and Yang H (2011). A role for oxysterol-binding protein-related protein 5 in endosomal cholesterol trafficking. J. Cell Biol 192, 121–135. [PubMed: 21220512]

Eriksson I, Nath S, Bornefall P, Giraldo AM, and Öllinger K (2017). Impact of high cholesterol in a Parkinson's disease model: prevention of lysosomal leakage versus stimulation of α-synuclein aggregation. Eur. J. Cell Biol 96, 99–109. [PubMed: 28109635]

Fraldi A, Klein AD, Medina DL, and Settembre C (2016). Brain Disorders Due to Lysosomal Dysfunction. Annu. Rev. Neurosci 39, 277–295. [PubMed: 27090953]

Gelsthorpe ME, Baumann N, Millard E, Gale SE, Langmade SJ, Schaffer JE, and Ory DS (2008). Niemann-Pick type C1 I1061T mutant encodes a functional protein that is selected for endoplasmic reticulum-associated degradation due to protein misfolding. J. Biol. Chem 283, 8229–8236. [PubMed: 18216017]

Ghai R, Du X, Wang H, Dong J, Ferguson C, Brown AJ, Parton RG, Wu JW, and Yang H (2017). ORP5 and ORP8 bind phosphatidylinositol-4, 5-biphosphate (PtdIns(4,5)P 2) and regulate its level at the plasma membrane. Nat. Commun. 8, 757. [PubMed: 28970484]

Ghezzi F, Monni L, and Nistri A (2018). Functional up-regulation of the M-current by retigabine contrasts hyperexcitability and excitotoxicity on rat hypoglossal motoneurons. J. Physiol 596, 2611–2629. [PubMed: 29736957]

Gulshan K, Brubaker G, Conger H, Wang S, Zhang R, Hazen SL, and Smith JD (2016). PI(4,5)P2 Is Translocated by ABCA1 to the Cell Surface Where It Mediates Apolipoprotein A1 Binding and Nascent HDL Assembly. Circ. Res 119, 827–838. [PubMed: 27514935]

Gunthorpe MJ, Large CH, and Sankar R (2012). The mechanism of action of retigabine (ezogabine), a first-in-class K+ channel opener for the treatment of epilepsy. Epilepsia 53, 412–424. [PubMed: 22220513]

Hajdú P, Varga Z, Pieri C, Panyi G, and Gáspár R Jr. (2003). Cholesterol modifies the gating of Kv1.3 in human T lymphocytes. Pflugers Arch. 445, 674–682. [PubMed: 12632187]

Herz J, and Bock HH (2002). Lipoprotein receptors in the nervous system. Annu. Rev. Biochem 71, 405–434. [PubMed: 12045102]

Hilgemann DW, Feng S, and Nasuhoglu C (2001). The complex and intriguing lives of PIP_2 with ion channels and transporters. Sci. STKE 2001, re19. [PubMed: 11734659]

Hille B, Dickson EJ, Kruse M, Vivas O, and Suh BC (2015). Phosphoinositides regulate ion channels. Biochim. Biophys. Acta 1851, 844–856. [PubMed: 25241941]

Jentsch TJ (2000). Neuronal KCNQ potassium channels: physiology and role in disease. Nat. Rev. Neurosci 1, 21–30. [PubMed: 11252765]

Karten B, Peake KB, and Vance JE (2009). Mechanisms and consequences of impaired lipid trafficking in Niemann-Pick type C1-deficient mammalian cells. Biochim. Biophys. Acta 1791, 659–670. [PubMed: 19416638]

Lange Y, Ye J, Rigney M, and Steck T (2000). Cholesterol movement in Niemann-Pick type C cells and in cells treated with amphiphiles. J. Biol. Chem 275, 17468–17475. [PubMed: 10751394]

Laplante M, and Sabatini DM (2012). mTOR signaling in growth control and disease. Cell 149, 274–293. [PubMed: 22500797]

Lee SY, Choi HK, Kim ST, Chung S, Park MK, Cho JH, Ho WK, and Cho H (2010). Cholesterol inhibits M-type K^+ channels via protein kinase C-dependent phosphorylation in sympathetic neurons. J. Biol. Chem 285, 10939–10950. [PubMed: 20123983]

Li X, Saha P, Li J, Blobel G, and Pfeffer SR (2016). Clues to the mechanism of cholesterol transfer from the structure of NPC1 middle lumenal domain bound to NPC2. Proc. Natl. Acad. Sci. USA 113, 10079–10084. [PubMed: 27551080]

Lloyd-Evans E, Morgan AJ, He X, Smith DA, Elliot-Smith E, Sillence DJ, Churchill GC, Schuchman EH, Galione A, and Platt FM (2008). Niemann-Pick disease type C1 is a sphingosine storage disease that causes deregulation of lysosomal calcium. Nat. Med 14, 1247–1255. [PubMed: 18953351]

Lu F, Liang Q, Abi-Mosleh L, Das A, De Brabander JK, Goldstein JL, and Brown MS (2015). Identification of NPC1 as the target of U18666A, an inhibitor of lysosomal cholesterol export and Ebola infection. eLife 4, e12177. [PubMed: 26646182]

Luo J, Jiang L, Yang H, and Song BL (2017). Routes and mechanisms of post-endosomal cholesterol trafficking: a story that never ends. Traffic 18, 209–217. [PubMed: 28191915]

Maekawa M, and Fairn GD (2015). Complementary probes reveal that phosphatidylserine is required for the proper transbilayer distribution of cholesterol. J. Cell Sci 128, 1422–1433. [PubMed: 25663704]

Mesmin B, Bigay J, Moser von Filseck J, Lacas-Gervais S, Drin G, and Antonny B (2013). A four-step cycle driven by PI(4)P hydrolysis directs sterol/ PI(4)P exchange by the ER-Golgi tether OSBP. Cell 155, 830–843. [PubMed: 24209621]

Millard EE, Srivastava K, Traub LM, Schaffer JE, and Ory DS (2000). Niemann-pick type C1 (NPC1) overexpression alters cellular cholesterol homeostasis. J. Biol. Chem 275, 38445–38451. [PubMed: 10964915]

Millat G, Marçais C, Rafi MA, Yamamoto T, Morris JA, Pentchev PG, Ohno K, Wenger DA, and Vanier MT (1999). Niemann-Pick C1 disease: the I1061T substitution is a frequent mutant allele in patients of Western European descent and correlates with a classic juvenile phenotype. Am. J. Hum. Genet 65, 1321–1329. [PubMed: 10521297]

Nordestgaard LT, Tybjærg-Hansen A, Nordestgaard BG, and Frikke-Schmidt R (2015). Loss-of-function mutation in ABCA1 and risk of Alzheimer's disease and cerebrovascular disease. Alzheimers Dement. 11, 1430–1438. [PubMed: 26079414]

Park WD, O'Brien JF, Lundquist PA, Kraft DL, Vockley CW, Karnes PS, Patterson MC, and Snow K (2003). Identification of 58 novel mutations in Niemann-Pick disease type C: correlation with biochemical phenotype and importance of PTC1-like domains in NPC1. Hum. Mutat 22, 313–325. [PubMed: 12955717]

Praggastis M, Tortelli B, Zhang J, Fujiwara H, Sidhu R, Chacko A, Chen Z, Chung C, Lieberman AP, Sikora J, et al. (2015). A murine Niemann-Pick C1 I1061T knock-in model recapitulates the pathological features of the most prevalent human disease allele. J. Neurosci 35, 8091–8106. [PubMed: 26019327]

Purcell EK, Liu L, Thomas PV, and Duncan RK (2011). Cholesterol influences voltage-gated calcium channels and BK-type potassium channels in auditory hair cells. PLoS One 6, e26289. [PubMed: 22046269]

Rauniyar N, Subramanian K, Lavallée-Adam M, Martínez-Bartolomé S, Balch WE, and Yates JR 3rd. (2015). Quantitative Proteomics of Human Fibroblasts with I1061T Mutation in Niemann-Pick C1 (NPC1) Protein Provides Insights into the Disease Pathogenesis. Mol. Cell. Proteomics 14, 1734–1749. [PubMed: 25873482]

Romanenko VG, Fang Y, Byfield F, Travis AJ, Vandenberg CA, Rothblat GH, and Levitan I (2004). Cholesterol sensitivity and lipid raft targeting of Kir2.1 channels. Biophys. J 87, 3850–3861. [PubMed: 15465867]

Rome S, Lecomte V, Meugnier E, Rieusset J, Debard C, Euthine V, Vidal H, and Lefai E (2008). Microarray analyses of SREBP-1a and SREBP-1c target genes identify new regulatory pathways in muscle. Physiol. Genomics 34, 327–337. [PubMed: 18559965]

Schulze H, and Sandhoff K (2011). Lysosomal lipid storage diseases. Cold Spring Harb. Perspect. Biol 3, a004804. [PubMed: 21502308]

Suh BC, and Hille B (2002). Recovery from muscarinic modulation of M current channels requires phosphatidylinositol 4,5-bisphosphate synthesis. Neuron 35, 507–520. [PubMed: 12165472]

Telezhkin V, Reilly JM, Thomas AM, Tinker A, and Brown DA (2012). Structural requirements of membrane phospholipids for M-type potassium channel activation and binding. J. Biol. Chem 287, 10001–10012. [PubMed: 22303005]

Traynor-Kaplan A, Kruse M, Dickson EJ, Dai G, Vivas O, Yu H, Whittington D, and Hille B (2017). Fatty-acyl chain profiles of cellular phosphoinositides. Biochim. Biophys. Acta Mol. Cell. Biol. Lipids 1862, 513–522. [PubMed: 28189644]

Vanier MT (1999). Lipid changes in Niemann-Pick disease type C brain: personal experience and review of the literature. Neurochem. Res 24, 481–489. [PubMed: 10227680]

Vanier MT, and Latour P (2015). Laboratory diagnosis of Niemann-Pick disease type C: the filipin staining test. Methods Cell Biol. 126, 357–375. [PubMed: 25665455]

Vivas O, Castro H, Arenas I, Elías-Viñas D, and García DE (2013). PIP_2 hydrolysis is responsible for voltage independent inhibition of CaV2.2 channels in sympathetic neurons. Biochem. Biophys. Res. Commun 432, 275–280. [PubMed: 23396054]

von Eckardstein A, Chirazi A, Schuler-Lüttmann S, Walter M, Kastelein JJ, Geisel J, Real JT, Miccoli R, Noseda G, Höbbel G, and Assmann G (1998). Plasma and fibroblasts of Tangier disease patients are disturbed in transferring phospholipids onto apolipoprotein A-I. J. Lipid Res 39, 987–998. [PubMed: 9610765]

Wang H, Ma Q, Qi Y, Dong J, Du X, Rae J, Wang J, Wu WF, Brown AJ, Parton RG, et al. (2019). ORP2 Delivers Cholesterol to the Plasma Membrane in Exchange for Phosphatidylinositol 4, 5-Bisphosphate (PI(4,5)P2). Mol. Cell 73, 458–473.e7. [PubMed: 30581148]

Watanabe H, Nagata E, Kosakai A, Nakamura M, Yokoyama M, Tanaka K, and Sasai H (2000). Disruption of the epilepsy KCNQ2 gene results in neural hyperexcitability. J. Neurochem 75, 28–33. [PubMed: 10854243]

Yu W, Ko M, Yanagisawa K, and Michikawa M (2005). Neurodegeneration in heterozygous Niemann-Pick type C1 (NPC1) mouse: implication of heterozygous NPC1 mutations being a risk for tauopathy. J. Biol. Chem 280, 27296–27302. [PubMed: 15919659]

Zaika O, Lara LS, Gamper N, Hilgemann DW, Jaffe DB, and Shapiro MS (2006). Angiotensin II regulates neuronal excitability via phosphatidylinositol 4,5-bisphosphate-dependent modulation of Kv7 (M-type) K+ channels. J. Physiol 575, 49–67. [PubMed: 16777936]

Zhang H, Craciun LC, Mirshahi T, Rohács T, Lopes CM, Jin T, and Logothetis DE (2003). PIP(2) activates KCNQ channels, and its hydrolysis underlies receptor-mediated inhibition of M currents. Neuron 37, 963–975. [PubMed: 12670425]

Zhao K, and Ridgway ND (2017). Oxysterol-Binding Protein-Related Protein 1L Regulates Cholesterol Egress from the Endo-Lysosomal System. Cell Rep. 19, 1807–1818. [PubMed: 28564600]

Zhu L, Zhong M, Elder GA, Sano M, Holtzman DM, Gandy S, Cardozo C, Haroutunian V, Robakis NK, and Cai D (2015). Phospholipid dysregulation contributes to ApoE4-associated cognitive deficits in Alzheimer's disease pathogenesis. Proc. Natl. Acad. Sci. USA 112, 11965–11970. [PubMed: 26372964]

Highlights

- Loss of NPC1 function causes neurons to become hyperexcitable
- Intrinsic hyperexcitability is triggered by reduced KCNQ2/3 current
- Decrease of KCNQ2/3 current in NPC1 disease is caused by a reduction in PtdIns(4,5)P_2
- Loss of PtdIns(4,5)$P2$ in NPC1 disease occurs due to upregulation of the ABCA1 transporter

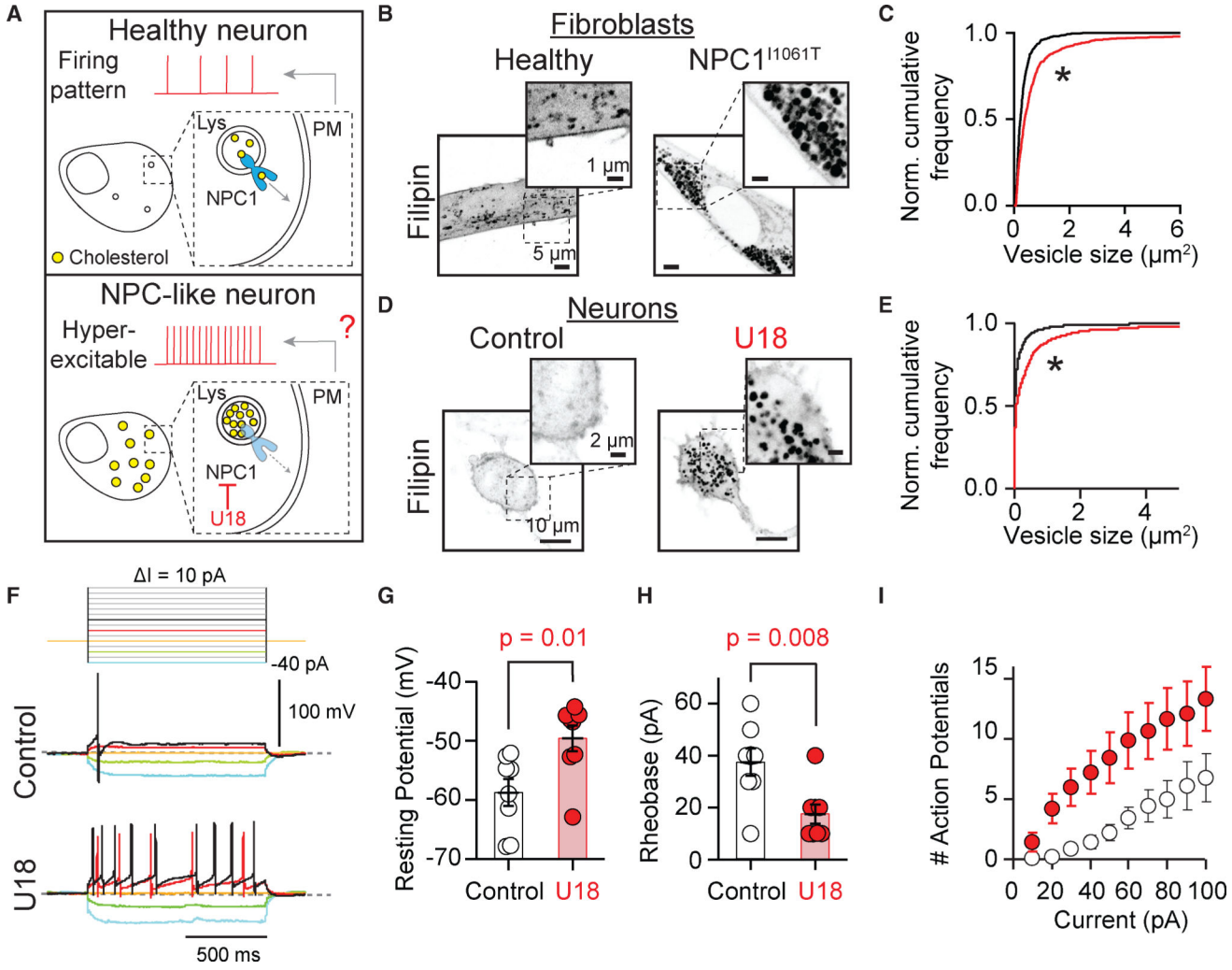

Figure 1. Pharmacological Inhibition of NPC1 Increases Neuronal Excitability

(A) Schematic of the hypothesis: lysosomal cholesterol efflux regulates neuron excitability.

(B) Inverted confocal micrographs of healthy (left) and NPC1^{I1061T} (right) fibroblasts fixed and stained with filipin. Insets show the accumulation of cholesterol within the lysosome lumen.

(C) Comparison of normalized cumulative frequencies of vesicle size between healthy (black, 16 cells, 777 vesicles) and NPC1^{I1061T} (red, 14 cells, 545 vesicles) fibroblasts. *p < 0.0005, Mann-Whitney-Wilcoxon test.

(D) Inverted confocal micrographs of control (left) and U18-treated (right; 1 μM, 18 h) sympathetic neurons fixed and stained with filipin.

(E) Comparison of normalized cumulative frequencies of vesicle size between neurons cultured without (black, 17 cells, 2,186 vesicles) and with (red, 20 cells,1,373 vesicles, *p < 0.0005, Mann-Whitney-Wilcoxon test) U18.

(F) Top: schematic of current injection protocol. Membrane potential was held at −65 mV, and current steps were given from −40 to 100 pA in 10-pA steps. Center: voltage traces from control neuron. Bottom: voltage traces from U18-treated neuron. Note that the U18-treated

neuron fires several APs with 40 pA current injection (bottom, black trace, 9 APs) compared to a neuron cultured without U18 (middle, black trace, 1 AP). Dotted lines: −65 mV.
(G) Summary of V_{rest} measured from neurons cultured without (empty circles, n = 8) and with (red circles, n = 8) U18.
(H) Quantification of the amount of current required to fire at least 1 AP (rheobase) in control (empty circles, n = 8) and U18-treated (red circles, n = 8) neurons.
(I) Comparison of the number of APs induced with increasing current injections in control (empty circles, n = 8) and U18-treated (red circles, n = 8) neurons. In all figures, average data are presented as mean ± SEM. See also Figure S1.

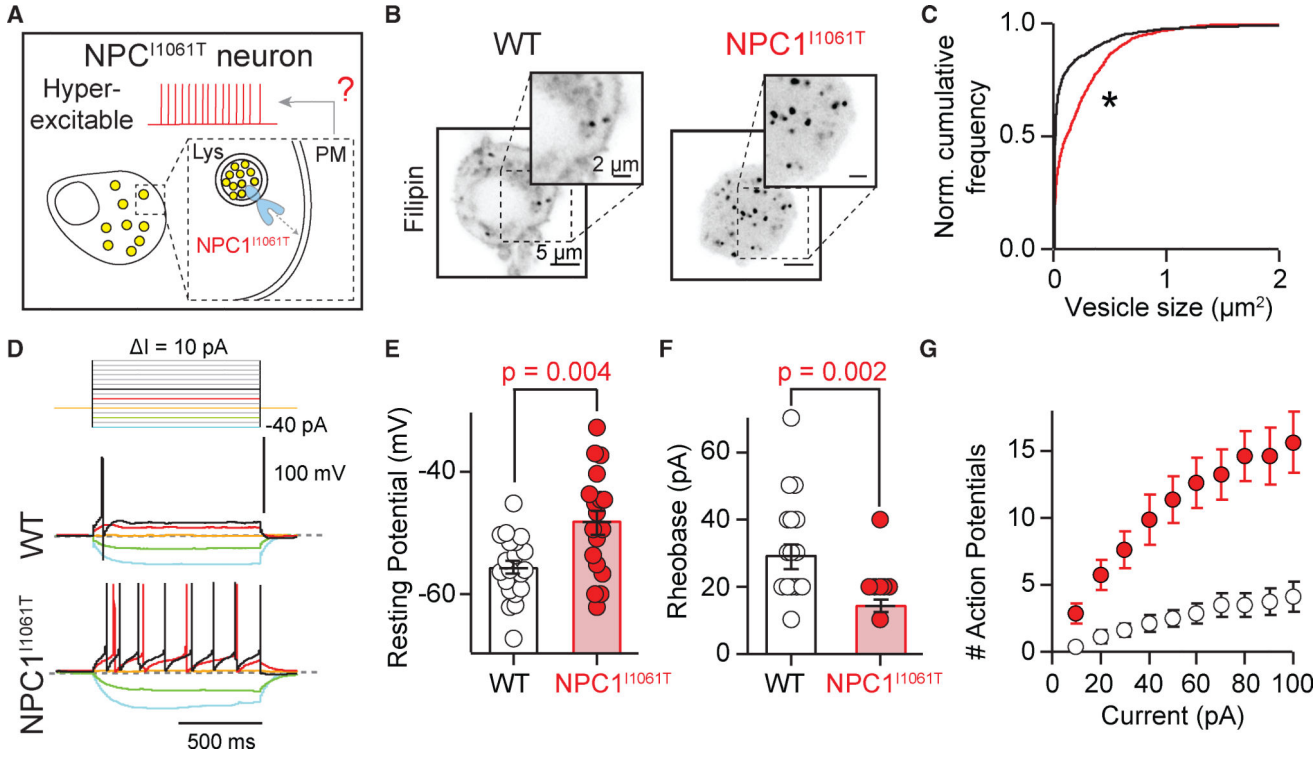

Figure 2. NPC1^{I1061T} Disease Neurons Are Hyperexcitable

(A) Schematic of the hypothesis: NPC1^{I1061T} disease neurons are hyperexcitable.

(B) Inverted confocal micrographs of WT (left) and NPC1^{I1061T} (right) mouse sympathetic neurons fixed and stained with filipin to show the accumulation of cholesterol.

(C) Comparison of normalized cumulative frequencies of vesicle size between wild-type (WT; black, 28 cells, 1,688 vesicles) and NPC1^{I1061T} (red, 24 cells, 1,043 vesicles, *p < 0.0005, Mann-Whitney-Wilcoxon test) neurons.

(D) Top: schematic of current injection protocol. Center: WT neuron fires 1 AP in response to 40 pA current injection (black trace). Bottom: NPC1^{I1061T} neuron fires several APs with 40 pA current injection (black trace, 9 APs). Dotted lines: −65 mV.

(E) Summary of V_{rest} measured from WT (empty circles, n = 20) or NPC1^{I1061T} (red circles, n = 18) neurons.

(F) Histogram comparing the rheobase in WT (empty circles, n = 20) and NPC1^{I1061T} (red circles, n = 18) neurons.

(G) Comparison of the number of APs induced with increasing current injections in WT (empty circles, n = 20) and NPC1^{I1061T} (red circles, n = 18) neurons.

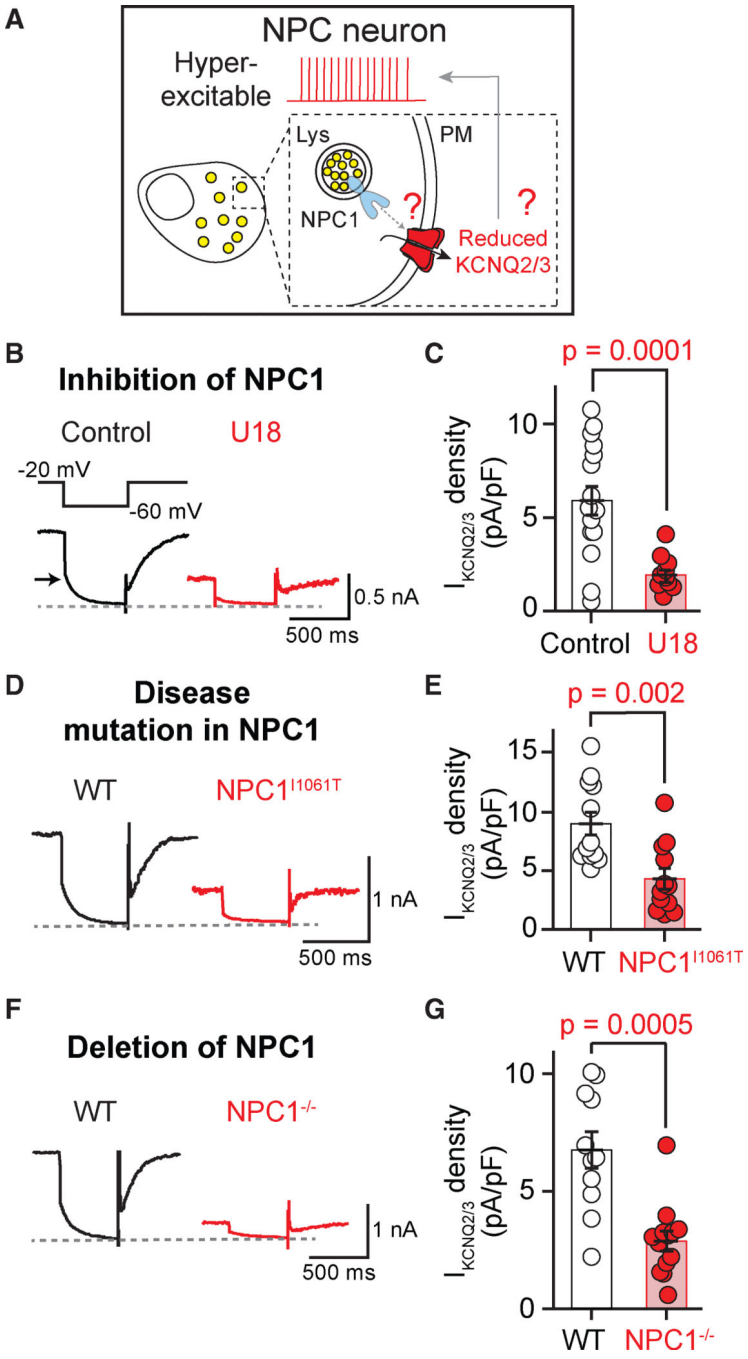

Figure 3. Loss of NPC1 Function Reduces $I_{KCNQ2/3}$

(A) Schematic of the hypothesis: reduction in $I_{KCNQ2/3}$ underlies $NPC1^{I1061T}$ hyperexcitability.

(B) Comparison of $I_{KCNQ2/3}$ recordings from neurons cultured overnight without (control) or with 1 μM U18. Arrow points toward the tail current, which was used to measure KCNQ2/3 current amplitude.

(C) Summary of $I_{KCNQ2/3}$ amplitude normalized to cell size from control (n = 16) and U18-treated (n = 11) neurons.

(D) $I_{KCNQ2/3}$ recordings from neurons isolated from WT or $NPC1^{I1061T}$ mice.
(E) Summary of $I_{KCNQ2/3}$ density from WT(n = 12) and $NPC1^{I1061T}$ (n =12) neurons.
(F) $I_{KCNQ2/3}$ recordings from neurons isolated from WT or knockout mice for NPC1 ($NPC1^{-/-}$).
(G) Summary of $I_{KCNQ2/3}$ density from WT (n = 11) and $NPC1^{-/-}$ (n = 12). Dotted lines in (B), (D), and (F): 0 pA.
See also Figure S2.

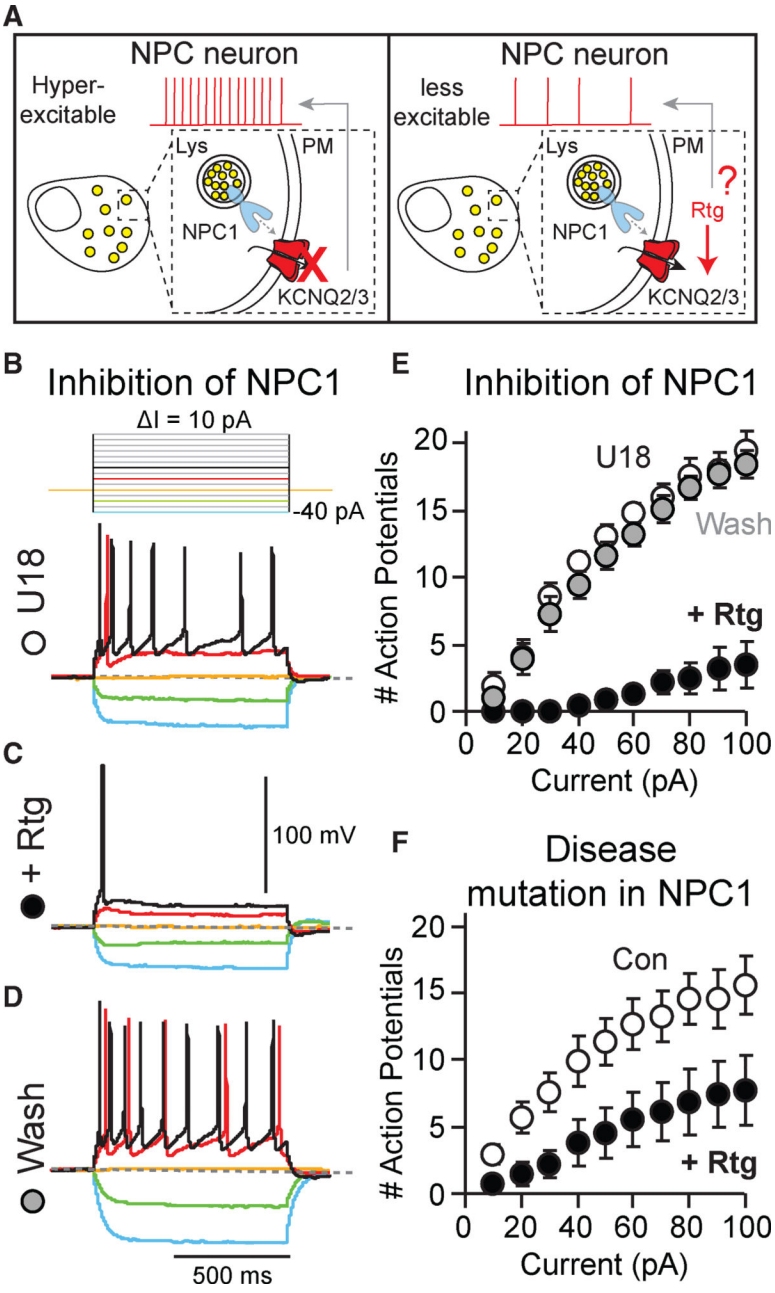

Figure 4. Opening KCNQ2/3 Channels Rescues NPC1^{I1061T} Neuron Excitability

(A) Schematic of the hypothesis: opening KCNQ2/3 channels rescues NPC1^{I1061T} hyperexcitability.

(B) Top: schematic of current injection protocol. Family of voltage recordings from a neuron treated overnight with 1 μM U18 (black trace, 7 APs).

(C) Family of voltage recordings from the same neuron as in (B), but after the application of 10 μM retigabine (Rtg; black trace, 1 AP).

(D) Family of voltage recordings from the same neuron as in (B) and (C) following 3 min of retigabine washout (black trace, 9 APs). Dotted lines in (B), (C), and (D): −65 mV.

(E) Comparison of the number of APs induced with increasing current injections from neurons treated with U18 (empty circles), after retigabine application (Rtg, black circles), and following washout (gray circles). Data from eight cells collected from three independent experiments. At 100 pA injected current, $p < 0.0001$ for U18 versus retigabine, $p = 0.5$ for U18 versus washout, and $p < 0.0001$ for retigabine versus washout.

(F) Comparison of the number of APs fired per unit of injected current from$NPC1^{I1061T}$ mouse neurons before (empty circles) and after (black circles) retigabine application. Data from 14 cells collected from 3 independent experiments. At 100 pA, $NPC1^{I1061T}$: 16 ± 2 APs; $NPC1^{I1061T}$ + retigabine: 8 ± 3, $p = 0.02$.

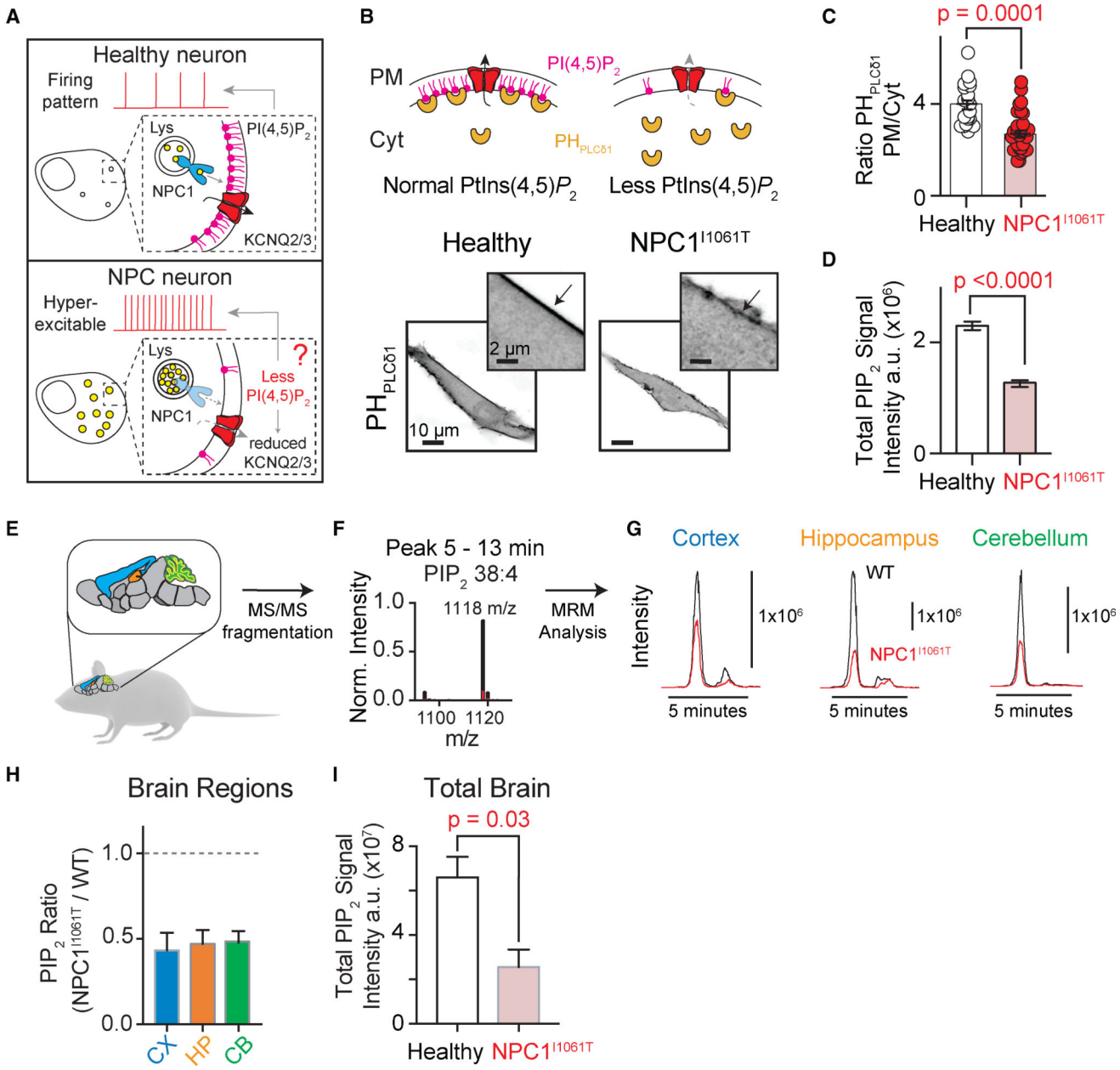

Figure 5. Plasma Membrane PtdIns(4,5)P_2 Is Reduced in NPC1 Disease

(A) Schematic of the hypothesis: decreased $I_{KCNQ2/3}$ density is due to reduced PM PtdIns(4,5)P_2.

(B) Top: diagram illustrating PH_{PLCd1} as a PtdIns(4,5)P_2 biosensor. Bottom: inverted confocal micrographs of healthy (left) and $NPC1^{I1061T}$ (right) patient fibroblasts transfected with $PH_{PLC\delta1}$. Insets show reduced intensity of $PH_{PLC\delta1}$ at the PM of $NPC1^{I1061T}$ patient fibroblasts.

(C) Comparison of the ratio of $PH_{PLC\delta1}$ fluorescence intensity at the PM to the cytoplasm (Cyt) in healthy (n = 21) and $NPC1^{I1061T}$ fibroblasts (n = 28, p = 0.0001).

(D) UPLC-MS/MS PtInsP_2 measurements from healthy and $NPC1^{I1061T}$ patient fibroblasts (n = 5 independent cultures, p < 0.0001).

(E) Mouse brain regions used for experiments: blue, cortex; orange, hippocampus; and green, cerebellum.
(F) Profile of the *m/z* ratio for the most abundant PtInsP_2 isoform 38:4.
(G) Comparison of elution profiles of 38:4 PtInsP_2 in WT and NPC1^{I1061T} mice from each brain region (n = 3 mice).
(H) Comparison of the ratio of total PtInsP_2 in NPC1^{I1061T} to WT mice across brain regions. Total PtInsP_2 includes all isoforms of PtInsP_2 (e.g., 38:4, 36:2, 34:1).
(I) Summary of UPLC-MS/MS PtInsP_2 measurements from WT and NPC1^{I1061T} brains (n = 3 animal, p = 0.03).
See also Figure S3.

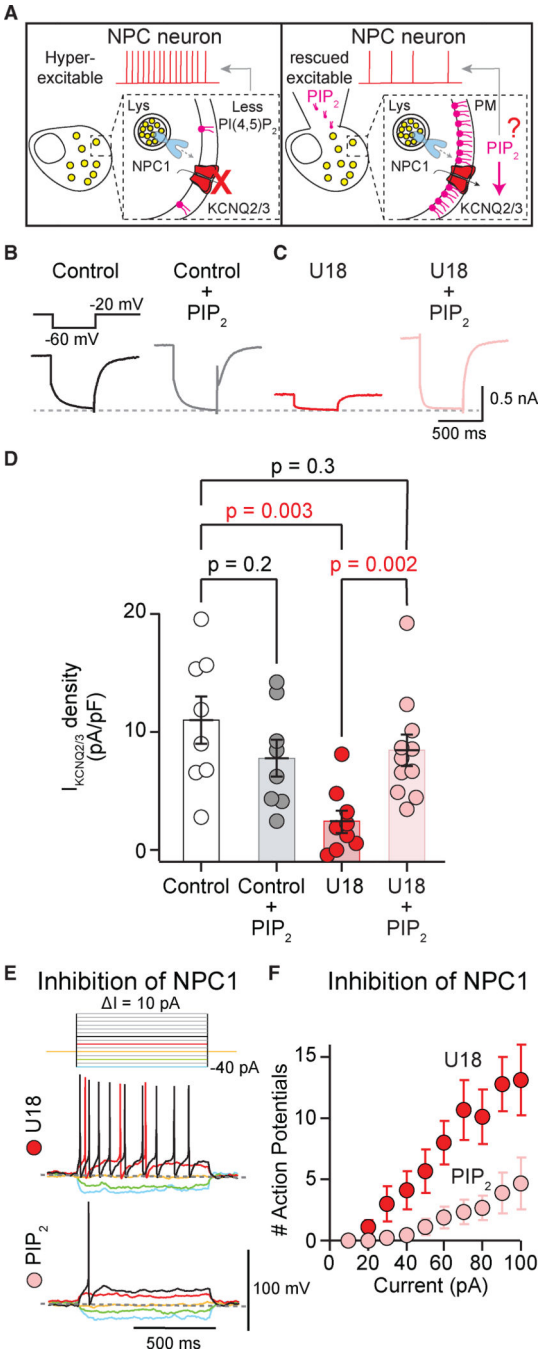

Figure 6. Exogenous Application of PtdIns(4,5)P_2 Rescues Both $I_{KCNQ2/3}$ and Excitability

(A) Schematic of the hypothesis: exogenous application of diC8-PtdIns(4,5)P_2 rescues $I_{KCNQ2/3}$ density and excitability.

(B) Comparison of $I_{KCNQ2/3}$ recordings from neurons cultured overnight without U18 (control) and patch without (black) or with (gray) 30 μM diC8-PtdIns(4,5)P_2. Inset: protocol used to isolate $I_{KCNQ2/3}$. Dotted line: 0 pA.

(C) Comparison of $I_{KCNQ2/3}$ recordings from neurons cultured overnight with 1 μM U18 and patched without (red) or with (pink) 30 μM diC8-PtdIns(4,5)P_2.

(D) Summary of $I_{KCNQ2/3}$ amplitude normalized to cell size from control (n = 8, empty), control patch with diC8-PtdIns(4,5)P (n = 8, gray), U18-treated neurons (n = 9, red), and U18-treated neurons patch with diC8-PtdIns(4,5)P_2 (n = 11, pink).

(E) Top: schematic of current injection protocol. Center: family of voltage recordings shows a U18-treated neuron firing 9 APs with 40 pA current injection (black trace). Bottom: family of voltage recordings shows a U18-treated neuron patched with 30 μM diC8-PtdIns(4,5)P_2 in the recording pipette firing only 1 AP (bottom, black trace). U18-treated neuron patched with diC8-PtdIns(4,5)P_2 does not fire any APs with less current injected (red trace). Dotted lines: −65 mV.

(F) Comparison of the number of APs induced with increasing current injections in U18-treated neurons (red, n = 6) and U18-treated neurons patched with diC8-PtdIns(4,5)P_2 (pink, n = 8).

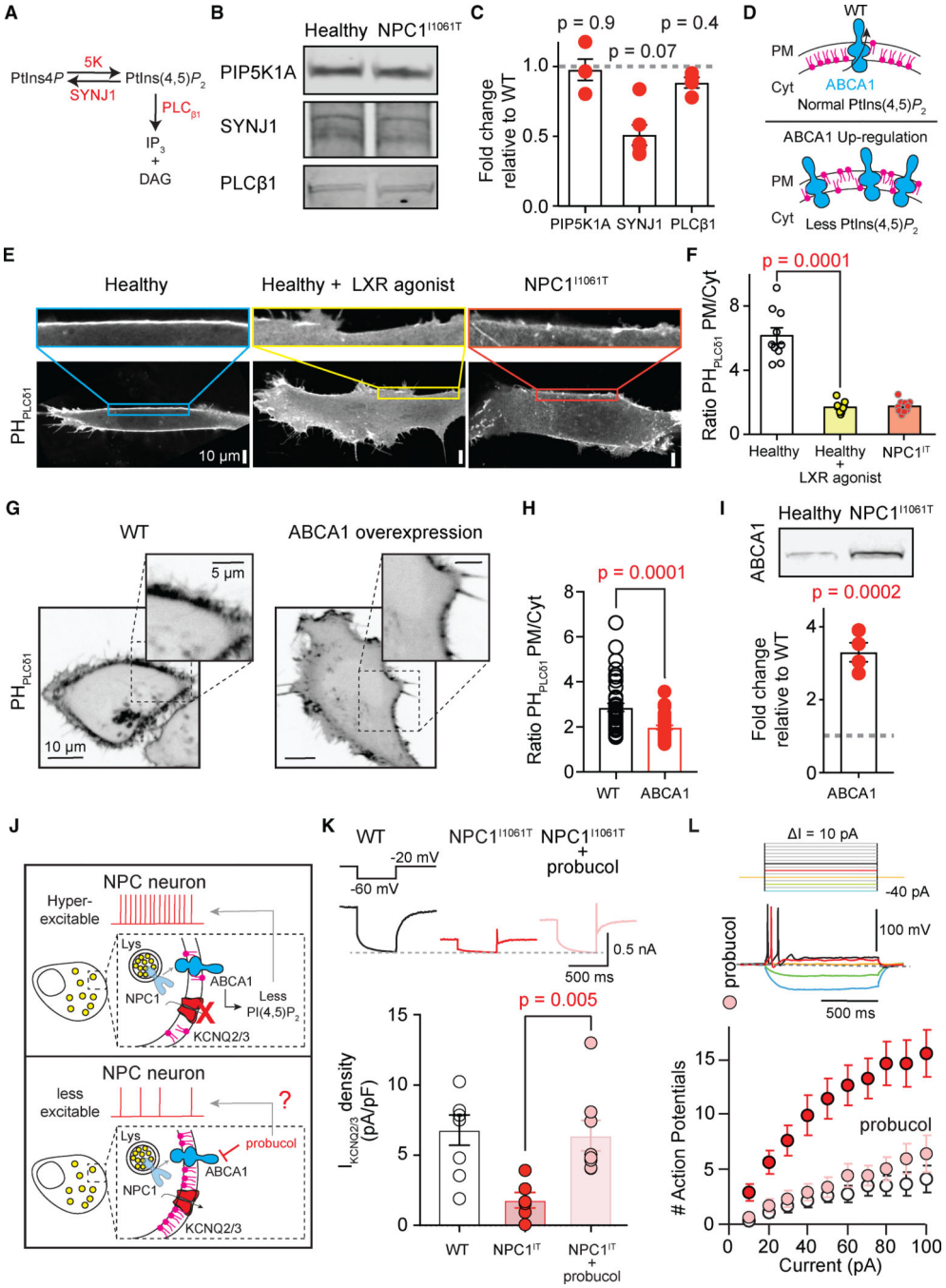

Figure 7. Upregulation of ABCA1 in NPC1 Disease Decreases PtdIns(4,5)P_2 and Leads to Hyperexcitability

(A) Schematic of PtdIns(4,5)P_2 synthesis. Relevant enzymes are in red.

(B) Blot stained for PtdIns(4,5)P_2 metabolizing enzymes PIP5K1A, SYNJ1, and PLC$_{\beta 1}$ from cerebellums collected from NPC1^{I1061T} and WT littermate mice.

(C) Summary of fold change of protein abundance in NPC1^{I1061T} cerebellum relative to WT (n = 4 blots from different mice).

(D) Schematic of hypothesis: upregulation of ABCA1 reduces PtdIns(4,5)P_2 levels.

(E) Confocal micrographs of healthy (left) and NPC1^{I1061T} (right) fibroblasts transfected with $PH_{PLC\delta1}$. Some healthy fibroblasts were treated with 1 μM T0901317, an LXR agonist, overnight (center). Insets show the reduced intensity of $PH_{PLC\delta1}$ at the PM from healthy fibroblasts treated with LXR agonist.

(F) Comparison of the ratio of $PH_{PLC\delta1}$ fluorescence intensity at the PM relative to the Cyt in healthy (empty, n = 13), healthy treated with LXR agonist (yellow, n = 15), and NPC1^{I1061T} fibroblasts (red, n = 10).

(G) Inverted confocal micrographs of HeLa cells with endogenous levels of ABCA1 (WT, left) and overexpressed levels of ABCA1 (ABCA1, right) transfected with $PH_{PLC\delta1}$. Insets show the reduced intensity of $PH_{PLC\delta1}$ at the PM of HeLa cells with upregulated levels of ABCA1.

(H) Comparison of the ratio of $PH_{PLC\delta1}$ fluorescence intensity at the PM to the Cyt in WT (n = 40) and ABCA1 HeLa cells (n = 33).

(I) Top: blot stained for ABCA1 from cerebellum collected from NPC1^{I1061T} and WT littermate mice. Bottom: summary of fold change of ABCA1 abundance in NPC1^{I1061T} cerebellum relative to WT (n = 4 blots from different mice).

(J) Schematic of the hypothesis: inhibition of ABCA1 in NPC neurons rescues current density and excitability.

(K) Inset: protocol used to isolate KCNQ2/3 current. Comparison of KCNQ2/3 current recordings from neurons isolated from WT (black) and NPC1^{I1061T} (red) mice. Some neurons isolated from NPC1^{I1061T} were treated with 10 μM probucol (pink). Dotted line: 0 pA. Bottom: summary of KCNQ2/3 current density from WT (n = 8, empty), NPC1^{I1061T} (n = 6, red), and NPC1^{I1061T} treated with probucol (n = 8, pink).

(L) Top: schematic of current injection protocol. Center: family of voltage recordings shows a probucol-treated NPC1^{I1061T} neuron firing 2 APs with 40 pA current injection (black trace). Dotted line: −65 mV. Bottom: comparison of the number of APs induced with increasing current injections in probucol-treated NPC1^{I1061T} neurons (pink, n = 9) and WT and NPC1^{I1061T} neurons (same data as Figure 2).

See also Figures S4, S5, S6, and S7.

KEY RESOURCES TABLE

REAGENT or RESOURCE	SOURCE	IDENTIFIER
Antibodies		
Rabbit monoclonal anti-NPC1	ABCAM	Cat # ab134113; RRID: AB_2734695
Rabbit polyclonal anti-KCNQ2	ABCAM	Cat # ab22897; RRID: AB_775890
Mouse monoclonal anti-B-actin	Thermo Scientific	Cat # MA1–91399; RRID: AB_2273656
Goat anti-rabbit	LI_COR biosciences	Cat # P/N 926–68071; RRID: AB_10956389
Goat anti-mouse	LI_COR biosciences	Cat # P/N 925–32210; RRID: AB_2687825
Mouse anti-ABCA1	ABCAM	Cat # Ab18180; RRID: AB_444302
Rabbit polyclonal anti-PIP5K1A	Cell Signaling Technology	Cat # 9693; RRID: AB_2164698
Rabbit polyclonal anti-SYNJ1	SIGMA	Cat # HPA011916; RRID: AB_1857692
Rabbit monoclonal anti-PLC beta 1	ABCAM	Cat # Ab182359
Chemicals, Peptides, and Recombinant Proteins		
Rabbit polyclonal anti-ORPL2	Proteintech	Cat # 14751–1-AP; RRID: AB_2156092
DiC8-PtdIns(4,5)P_2	Avanti Polar Lipids	Cat # 850185
PtdIns(4,5)P_2 standard	Avanti Polar Lipids	Cat # LM-1904
U18666A	SIGMA	Cat # 662015
Retigabine	APExBIO	Cat # A3758
Probucol	Fisher	Cat # 15637105
LXR agonist, T0901317	SIGMA	Cat # 575310
Experimental Models: Cell Lines		
Human: Healthy Fibroblasts or wild type Fibroblasts: From a healthy male	Coriell Institute	Cat # GM05659; RRID: CVCL_7434
Human: NPC1^{I1061T} Fibroblasts: From a male patient with mutation in NPC1 (I1061T)	Coriell Institute	Cat # GM18453; RRID: CVCL_DA78
Human: HeLa cells	Provided by Dr. Alan Remaley (NHLBI)	N/A
Human: ABCA1-GFP HeLa cells	Provided by Dr. Alan Remaley (NHLBI)	N/A
Experimental Models: Organisms/Strains		
Mouse: (NPC1$^{-/-}$): BALB/c strain knock-out of NPC1, NPC^{NIH}, NPC1^{m1N}	Provided by Dr. Daniel Ory (Washington University Saint Louis)	RRID: IMSR_JAX:003092
Mouse: NPC1^{I1061T}: C57BL/6 Strain knock-in of NPC1I1061T	Provided by Dr. Daniel Ory. Praggastis et al., 2015	N/A
Mouse: wild type (WT): C57BL/6	Jackson Laboratory	RRID: IMSR_JAX:000664
Oligonucleotides		
NPC1^{I1061T} allele 5′-tgatctgcacacttggaaccgag-3′ forward	Praggastis et al., 2015	N/A
NPC1^{I1061T} allele 5′-cactgccttgagcagcatctcag-3′ reverse	Praggastis et al., 2015	N/A
siRNA targeting sequence: ABCA1 #1: 5′-GCUCUUUCCUGAAUGUCAUCAACAA-3′	This paper	N/A

REAGENT or RESOURCE	SOURCE	IDENTIFIER
siRNA targeting sequence: ABCA1 #2: 5′-CUACUACCUGACCUUGGUCAAGAAA-3′	This paper	N/A
siRNA targeting sequence: ABCA1 #3: 5′-CUUAUUUUUCUAGUCAGUAAACATT-3′	This paper	N/A
Recombinant DNA		
$PH_{PLC\delta1}$ plasmid	Provided by Dr. Kees Jalink (the Netherlands Cancer Institute)	N/A
Software and Algorithms		
ImageJ	ImageJ	RRID: SCR_003070
IGOR Pro	WaveMetrics	RRID: SCR_000325
Prism	GraphPad	RRID: SCR_002798
Microsoft Excel	Microsoft	RRID: SCR_016137
Masslynx	Waters	RRID: SCR_014271